Electronic Supplementary Information for:

Intersystem crossing and spin dynamics of thionated perinones: combined steady-state/transient optical and electron paramagnetic resonance spectral analysis

Jieyu Tang,‡[a] Sveva Linarello,‡[b] Wenbin Chen,‡[c] Yuqi Hou,[d] Yanran Wu,[a] Jianzhang Zhao,*[a] Antonio Barbon,*[b] Antonio Toffoletti,*[b] Bernhard Dick*[e] and Ming-De Li*[c]

[a] State Key Laboratory of Fine Chemicals, Frontier Science Center for Smart Materials, School of Chemical Engineering, Dalian University of Technology, Dalian 116024, P. R. China. *E–mail: zhaojzh@dlut.edu.cn (J.Z.)

[b] Dipartimento di Scienze Chimiche, Università degli Studi di Padova35131 Padova, Italy. *E-mail: antonio.barbon@unipd.it (A.B.) and antonio.toffoletti@unipd.it (A.T.)

[c] Department of Chemistry and Key Laboratory for Preparation and Application of Ordered Structural Materials of Guangdong Province, Shantou University, Shantou 515063, P. R. China. *E-mail: mdli@stu.edu.cn (M.L.)

[d] School of Chemical Engineering, Ocean and Life Sciences, Dalian University of Technology, Panjin 124221, P. R. China.

[e] Lehrstuhl für Physikalische Chemie, Institut für Physikalische und Theoretische Chemie, Universität Regensburg, Regensburg 93053, Germany. *Email: Bernhard.Dick@chemie.uni-regensburg (B.D.)

‡ These authors contributed equally to this work.

Contents

1. General Information and synthesis ……Page S3

2. NMR and HRMS spectra of compounds ……Page S8

3. UV-vis absorption and fluorescence emission spectra ……Page S17

4. Fluorescence Lifetime ……Page S20

5. Electrochemical and spectroelectrochemical study ……Page S23

6. Femtosecond transient absorption spectra……Page S26

7. Nanosecond transient absorption spectra……Page S32

8. Time-resolved electron paramagnetic resonance spectroscopy……Page S38

9. Theoretical computations ……Page S41

10. References ……Page S49

1. General Information and Synthesis

General method

All chemicals used in synthesis were analytically pure and were used as received. Solvents were dried prior to use. The UV-vis spectra were recorded with a UV2550 spectrophotometer (Shimadzu Ltd., Japan). Fluorescence emission spectra were recorded with an FS5 spectrofluorometer (photon counting detection method. Edinburgh Instruments, UK). Fluorescence lifetimes of compounds were measured with an OB920 luminescence lifetime spectrometer (Edinburgh Instruments, UK) and a EPL picosecond pulsed laser was used for excitation. The time-correlated single photon counting (TCSPC) was used. Fluorescence quantum yields (Φ_F) were measured by using an absolute photoluminescence quantum yield spectrometer (Quantaurus-QY Plus C13534-11, Hamamatsu Ltd., Japan).

1.1. Electrochemical studies. Cyclic voltammetry was performed with a CHI610D electrochemical workstation (CHI instruments, Inc., Shanghai, China). The counter electrode is a platinum electrode; a glassy carbon electrode was used as the working electrode. The ferrocenium/ferrocene (Fc^+/Fc) redox couple was used as an internal reference. $Bu_4N[PF_6]$ was used as the supporting electrolyte, and the $Ag/AgNO_3$ (0.1 M in dichloromethane, DCM) couple was used as the reference electrode. Sample solutions were deaerated with N_2 for *ca.* 15 min before measurement, and the N_2 atmosphere was kept during the measurement.

1.2. Nanosecond transient absorption spectroscopy. The nanosecond transient absorption spectra were recorded on a LP980 laser flash photolysis spectrometer (Edinburgh Instruments, UK). The sample solutions were deaerated with N_2 for 15 min before measurement. The samples were excited with nanosecond pulsed laser (Surelite I-10, USA; the wavelength is tuneable in the range of 210 – 2400 nm). The typical laser power is *ca.* 10 mJ per pulse. The data were processed by L900 software. For the triplet-triplet energy transfer study, NI-Br was used as a triplet photosensitizer and perinones as the triplet energy acceptor to obtain the triplet lifetime of perinones which are lack of ISC ability.

1.3 Femtosecond transient absorption spectroscopy. The femtosecond transient absorption spectroscopy (fs-TA) spectral study was performed with a setup based on a femtosecond Ti: Sapphire regenerative amplifier laser system (Coherent, Astrella-Tunable-F-1k) and femtosecond transient absorption spectrometer system (Ultrafast Systems, Helios Fire). The signal is monitored by a white-light continuum (320–800 nm) in a CaF_2 crystal and then this probe beam was split into two parts before traversing the sample. One probe laser beam with spot size 7.9×10^3 μm^2 goes through the

sample, while the other probe laser beam goes to the reference spectrometer to monitor the fluctuations in the probe beam intensity. The instrument response function was determined to be *ca.* 120 fs. For the experiments described in this study, the sample solution was excited by the 300 nm and 400 nm pump beam with a power of 0.3 mW (37.9 μJ/cm^2) (from TOPAS), respectively. The data were stored as three-dimensional (3D) wavelength-time-absorbance matrices that were exported for use with the fitting software. The data were analysed with a global fitting procedure using the GLOTARAN package and applying a linear sequential model.[1]

1.4. TREPR spectroscopy. The prepared solutions of the compound to be analysed were taken into a quartz tube (3 mm i.d.) and degassed under a vacuum to remove dissolved gas by the freeze−pump−thaw cycle. An Elexsys Burker EPR spectrometer with a dielectric cavity in an Oxford CF935 cryostat, having optical access to irradiate the sample with a pulsed laser (Quantel Nd:YAG; 5 ns duration), was used to analyze the samples.[2]

1.5. Theoretical computation

The geometries of the lowest triplet state were optimized with the unrestricted DFT method, the B3LYP functional, and the 6-31G(d) basis set,[3] using the Gaussian 16 programs.[4]

The calculation of the ISC rate constants uses the time-correlation function method. This is based on a transformation of the Fermi-Golden-Rule expression into time domain, followed by analytic integration over all nuclear coordinates within the harmonic approximation. Formulas have been published by Niu et al.,[5] Etinski et al.,[6–8] Baiardi et al.,[9] and de Souza et al.[10] The equations for fluorescence given by the latter two are easily modified for ISC, and we used these formulas for our program. The formulas of de Souza are implemented in the ORCA [11,12] program suite and calculate the ISC rate constant for one fixed value of the energy gap. However, once the time-correlation function has been obtained, Fourier transform can produce the ISC rate constant as a function of the energy gap. Since the energy gap between singlet and triplet states is very often not known, this function is useful for estimating a range for the ISC rate constant.

This method calculates not only the Franck-Condon terms but also the Herzberg Teller contributions, which become important when the spin-orbit coupling matrix element (SOC-ME) becomes small or vanishes due to symmetry. Dushinsky rotation of the normal coordinates is also considered. The method requires the optimized geometries and hessian matrices of the initial and final states, the SOC-ME between these states, and the derivatives of the SOC-ME along all normal coordinates of the final state.

These data are produced in the ESD (electronic state dynamics) module of ORCA using TD-DFT.[10,13] In our application, we use the B3LYP functional and the def2-SVP basis set.

1.6. General procedure for preparation of thiocarbonyl compounds

To a mixture of carbonyl compounds (1 mmol) and Lawesson's reagent (2 mmol) were dissolved in *p*-xylene and the mixture was refluxed under a nitrogen atmosphere for 12 h. After the reaction mixture was cooled down to room temperature and the solvent was evaporated under reduced pressure, the residue was purified by column chromatography (silica gel, hexanes (HEX)/dichloromethane (DCM) = 4:1, v/v).[14,15]

Synthesis of target materials.

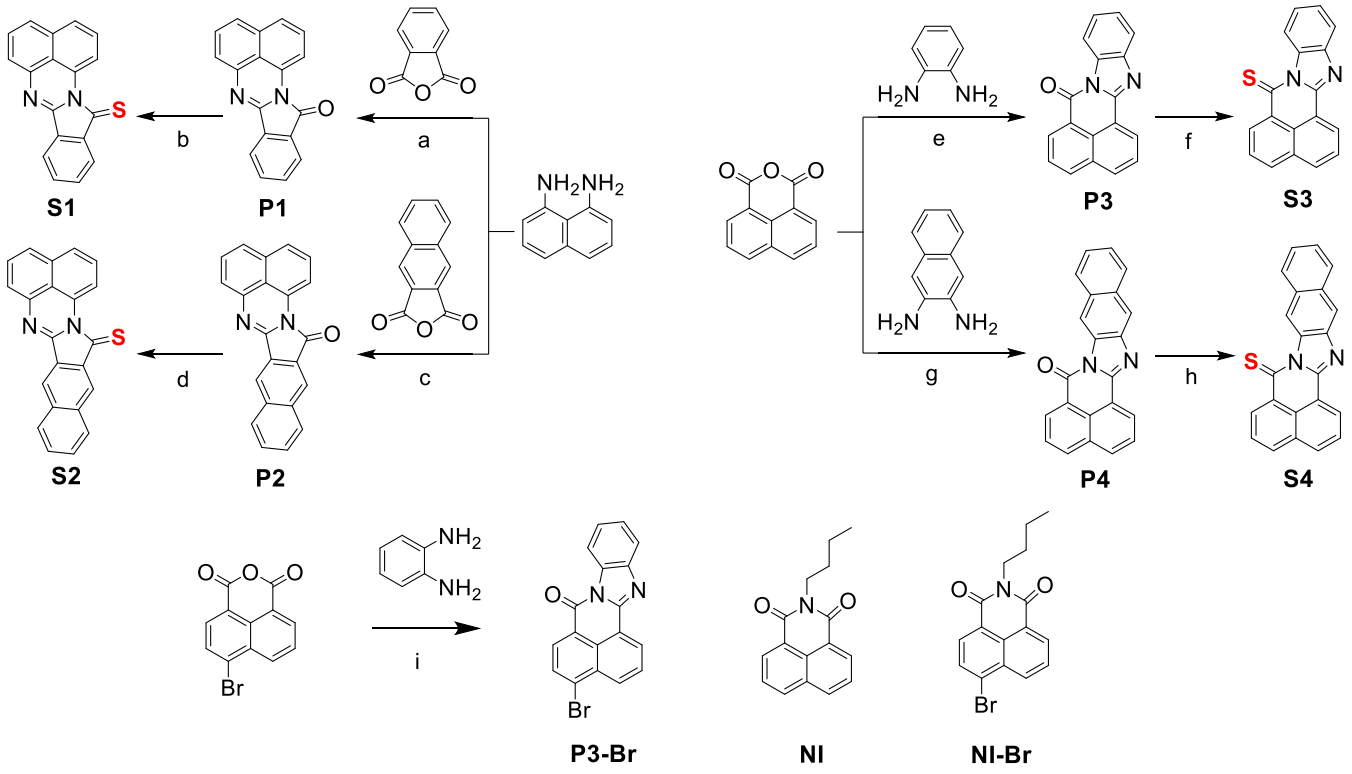

Scheme S1. Synthetic scheme for the thionated compound and the reference compounds are also presented. (a) TOL, CH_3COOH, reflux, 6 h, yield: 82%; (b) Lawesson's reagent, dry p-xylene, N_2, reflux, 18 h, yield: 28%; (c) is similar to (a), yield: 75%; (d) is similar to (b), yield: 10%; (e) Propionic acid, reflux, 2 h, yield: 54%; (f) is similar to (b), yield: 37%; (g) is similar to (e), yield: 56%; (h) is similar to (b) yield: 6%; (i) acetic acid, 24h, yield: 4%.

Compound S1[14]: red solid, yield: 28%. ^{1}H NMR (400 MHz, CD_2Cl_2) δ = 10.19 (d, 1H, *J* = 8.00 Hz), 8.14 (d, 2H, *J* = 6.88 Hz), 7.83 – 7.75 (m, 4H), 7.67 (d, 1H, *J* = 6.50 Hz), 7.61 – 7.54 (m, 2H). MS (APCI): calcd for $C_{18}H_{11}NS$ $[M+H]^+$, *m/z* 287.0637, found *m/z* 287.0642.

Compound S2[14]: red solid, yield: 10%. ^{1}H NMR (400 MHz, $CDCl_3$) δ = 10.23 (s, 1H), 8.65 (m, 2H), 8.11 (s, 2H), 7.67 – 7.54 (m, 7H). MS (APCI): calcd for $C_{22}H_{13}N_2S$ $[M+H]^+$, *m/z* 337.0794, found *m/z* 337.0798.

Compound S3[14]: orange solid, yield: 37%. ^{1}H NMR (400 MHz, DMSO) δ = 9.34 (d, 1H, *J* = 8.26 Hz), 9.04 (d, 1H, *J* = 7.63 Hz), 8.81 (d, 1H, *J* = 7.25 Hz), 8.53 (d, 1H, *J* = 8.00 Hz), 8.38 (d, 1H, *J* = 8.13 Hz), 7.92 – 7.88 (m, 3H), 7.60 – 7.56 (m, 1H), 7.52 – 7.49 (m, 1H). MS (APCI): calcd for $C_{18}H_{11}N_2S$ $[M+H]^+$, *m/z* 287.0637, found *m/z* 287.0639.

Compound S4[15]: red solid, yield: 6%. ^{1}H NMR (400 MHz, $CDCl_3$) δ = 10.05 (s, 1H), 9.18 (d, 1H, *J* = 7.63 Hz), 9.07 (d, 1H, *J* = 6.25 Hz), 8.36 (s, 1H), 8.26 (d, 1H, *J* = 8.00 Hz), 8.20 (d, 1H, *J* = 8.13 Hz), 8.11 – 8.03 (m, 2H), 7.85 – 7,77 (m, 2H), 7.58 – 7.52 (m, 2H). MS (APCI): calcd for $C_{22}H_{13}N_2S$ $[M+H]^+$, *m/z* 337.0794, found *m/z* 337.0802.

Compound P3-Br[16,17]: In a 100 mL round-bottom flask, 4-Bromo-1,8-naphthalic anhydride (1.0 g, 3.6 mmol), acetic acid (20 mL) and *o*-Phenylenediamine (475 mg, 4.4 mmol) were added, and the mixture was refluxed for 24 hours. Upon completion of the reaction, the mixture was poured into ice water, and the precipitate was filtered off. The product was purified through multiple recrystallizations with acetic acid to obtained a pure yellow crystal solid. 49 mg, yield: 4%.^{1}H NMR (400 MHz, $CDCl_3$) δ = 9.04 (d, 1H, *J* = 7.25 Hz), 8.63 (d, 1H, *J* = 7.88 Hz), 8.56 (d, 2H, *J* = 8.13 Hz), 8.14 (d, 1H, *J* = 8.00 Hz), 7.95 – 7.91 (m, 2H), 7.53 – 7.51 (m, 2H). HRMS (ESI): calcd for $C_{18}H_{10}BrN_2O$ $[M+H]^+$, *m/z* 348.9971, found *m/z* 348.9975.

Synthesis of Compound P1 and P2. [14] 1, 8-diaminaphthalene (4 mmol) and Phthalic anhydride or 2,3-Naphthalenedicarboxylic anhydride (4 mmol) were taken in toluene (20 mL) and acetic acid (2 mL). The mixture was refluxed for 6 h. After cooling down to room temperature, the crude product was extracted and filtered. Recrystallization in boiling toluene to obtain the pure product.

Compound P1: yellow solid, yield: 82%. ^{1}H NMR (400 MHz, $CDCl_3$) δ = 10.19 (d, 1H, *J* = 8.00 Hz), 8.14 (d, 2H, *J* = 6.88 Hz), 7.83 – 7.75 (m, 4H), 7.67 (d, 1H, *J* = 6.50 Hz), 7.61 – 7.54 (m, 2H). MS (APCI): calcd for $C_{18}H_{11}N_2O$ $[M+H]^+$, *m/z* 271.08, found *m/z* 271.1.

Compound P2: orange solid, yield: 75 %. ^{1}H NMR (400 MHz, $CDCl_3$) δ = 8.74 (s, 1H), 8.56 – 8.53 (m, 2H), 8.13 – 8.11 (m, 2H), 7.71 – 7.70 (m, 2H), 7.55 – 7.46 (m, 5H). HRMS (ESI): calcd for $C_{22}H_{13}N_2O$ $[M+H]^+$, *m/z* 321.1022, found *m/z* 321.1.

Compound P3 and P4. [15] 1,8-Napththalic anhydride (1 mmol) and diamino compounds (1.1 mmol) were taken in propionic acid (50 mL). The mixture was refluxed for 2 h. After cooling to room temperature, water was poured into the reaction mixture. The resulting precipitate was collected by filtration and washed with several portions of water to remove all the propionic acid. The crude product was recrystallized from boiling propionic acid to obtain the pure product.

Compound P3: yellow solid, yield: 54%. ^{1}H NMR (400 MHz, $CDCl_3$) δ = 8.84 (d, 1H, *J* = 7.25 Hz), 8.76 (dd, 1H, *J* = 7.25, 1.13 Hz), 8.58 – 8.52 (m, 1H), 8.25 (dd, 1H, *J* = 8.13, 1 Hz), 8,12 (d, 1H, *J* = 8.25 Hz), 7.911 – 7.86 (m, 1H), 7.82 – 7.76 (m, 2H), 7.52 – 7.45 (m, 2H). MS (APCI): calcd for $C_{18}H_{11}N_2O$ $[M+H]^+$, *m*/*z* 271.0866, found *m*/*z* 271.0866.

Compound P4: orange solid, yield: 56%. ^{1}H NMR (400 MHz, $CDCl_3$) δ = 9.19 (d, 1H, *J* = 6.38 Hz), 9.07 (s, 1H), 8.87 (d, 1H, *J* = 6.75 Hz), 8.41 (s, 1H), 8,34 (d, 1H, *J* = 8.00 Hz), 8.26 (d, 1H, *J* = 8.13 Hz), 8.12 – 8.05 (m, 2H), 7.92 – 7.87 (m, 2H), 7.58 – 7.54 (m, 2H). MS (ESI): calcd for $C_{22}H_{13}N_2O$ $[M+H]^+$, *m*/*z* 321.1023, found *m*/*z* 321.1023.

2. NMR and HRMS Spectra of compounds

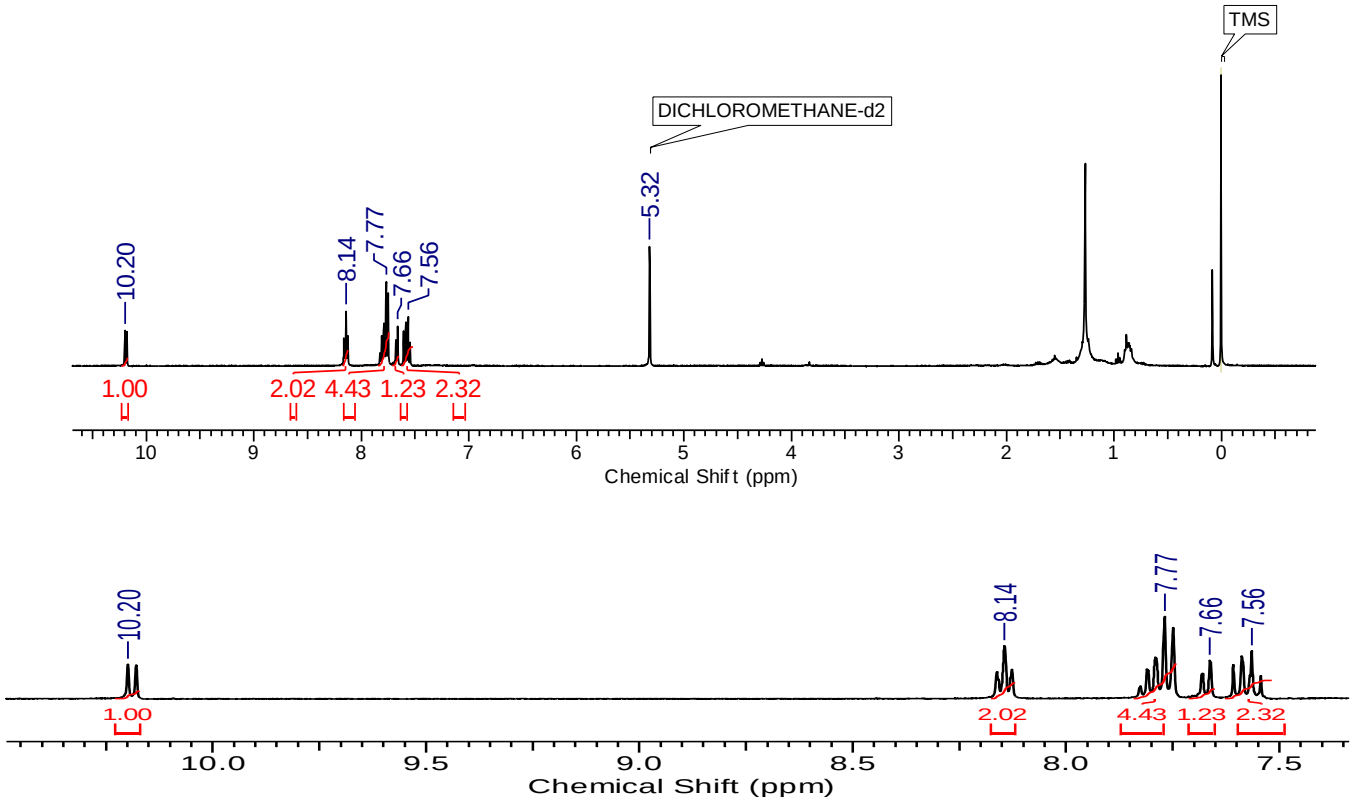

Fig. S1 ^{1}H NMR spectrum of **P1** ($CDCl_2$, 400 MHz).

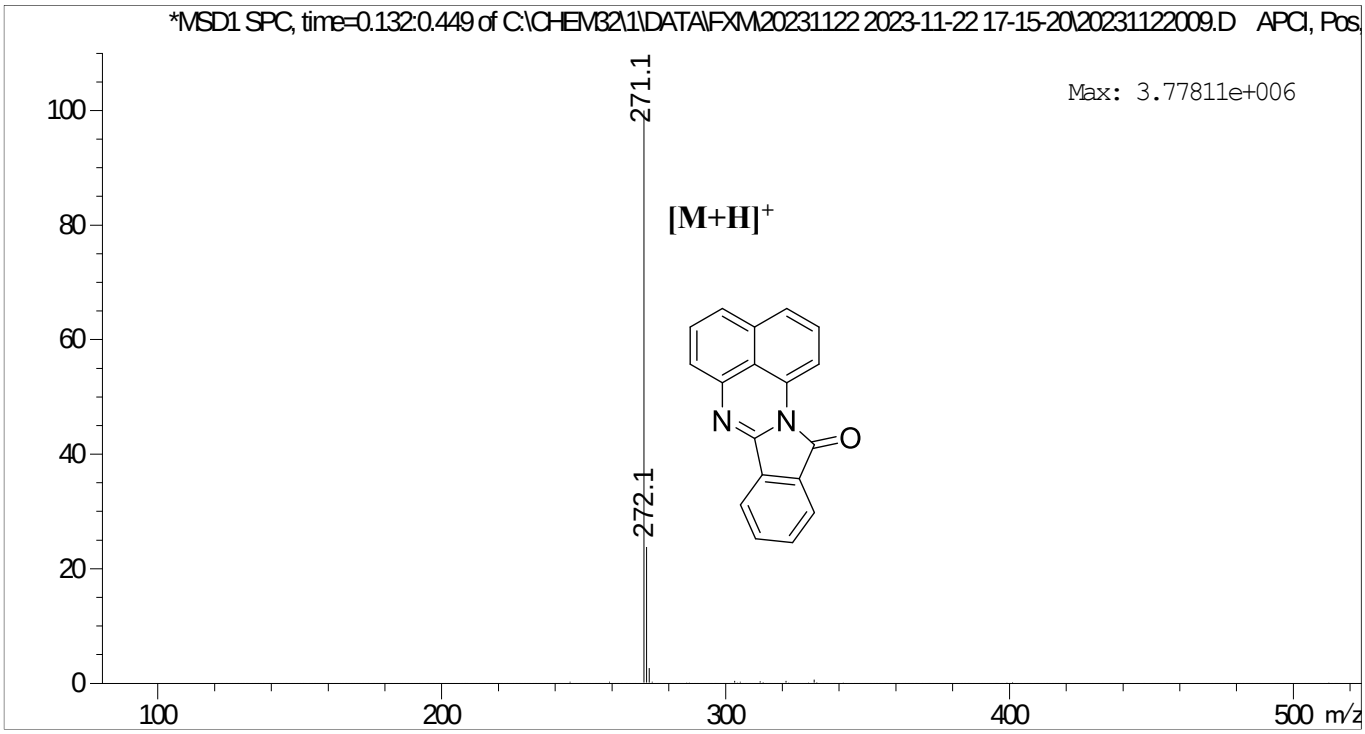

Fig. S2 APCI-MS of of **P1**.

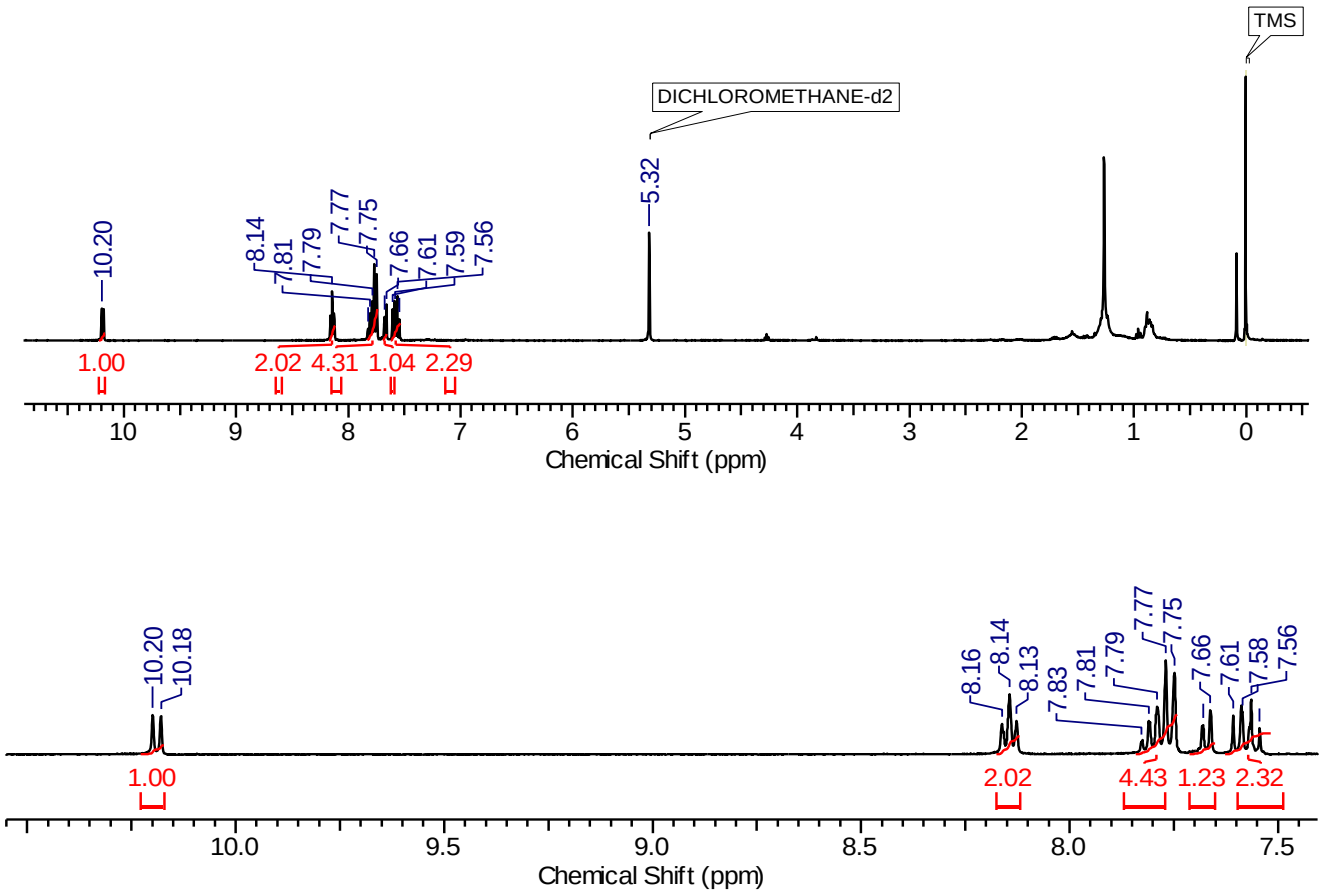

Fig. S3 ^{1}H NMR spectrum of **S1** (CD_2Cl_2, 400 MHz).

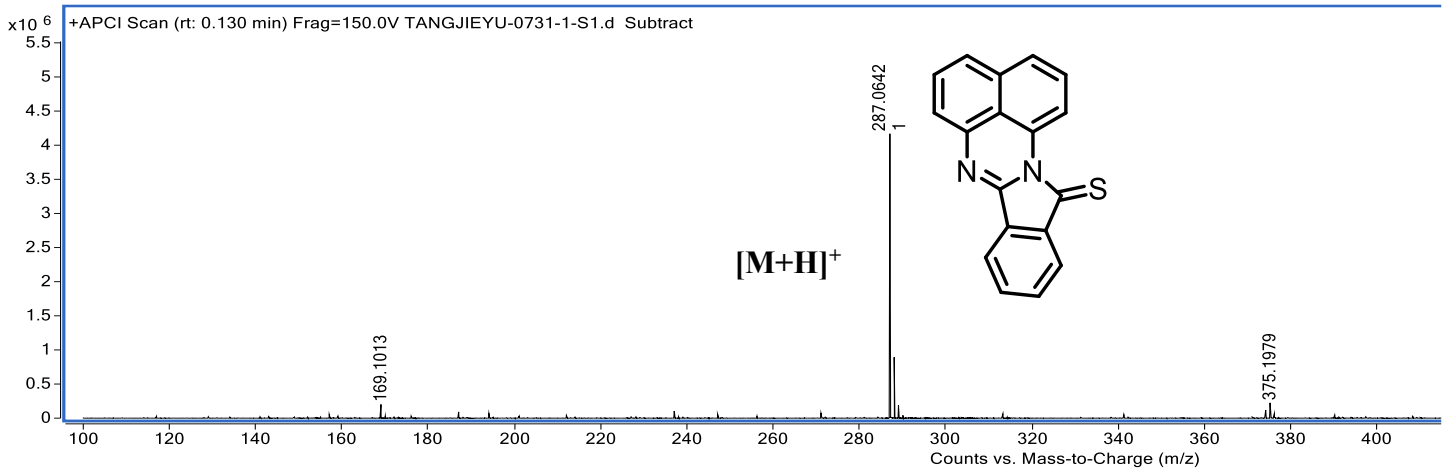

Fig. S4 APCI-MS of of **S1**.

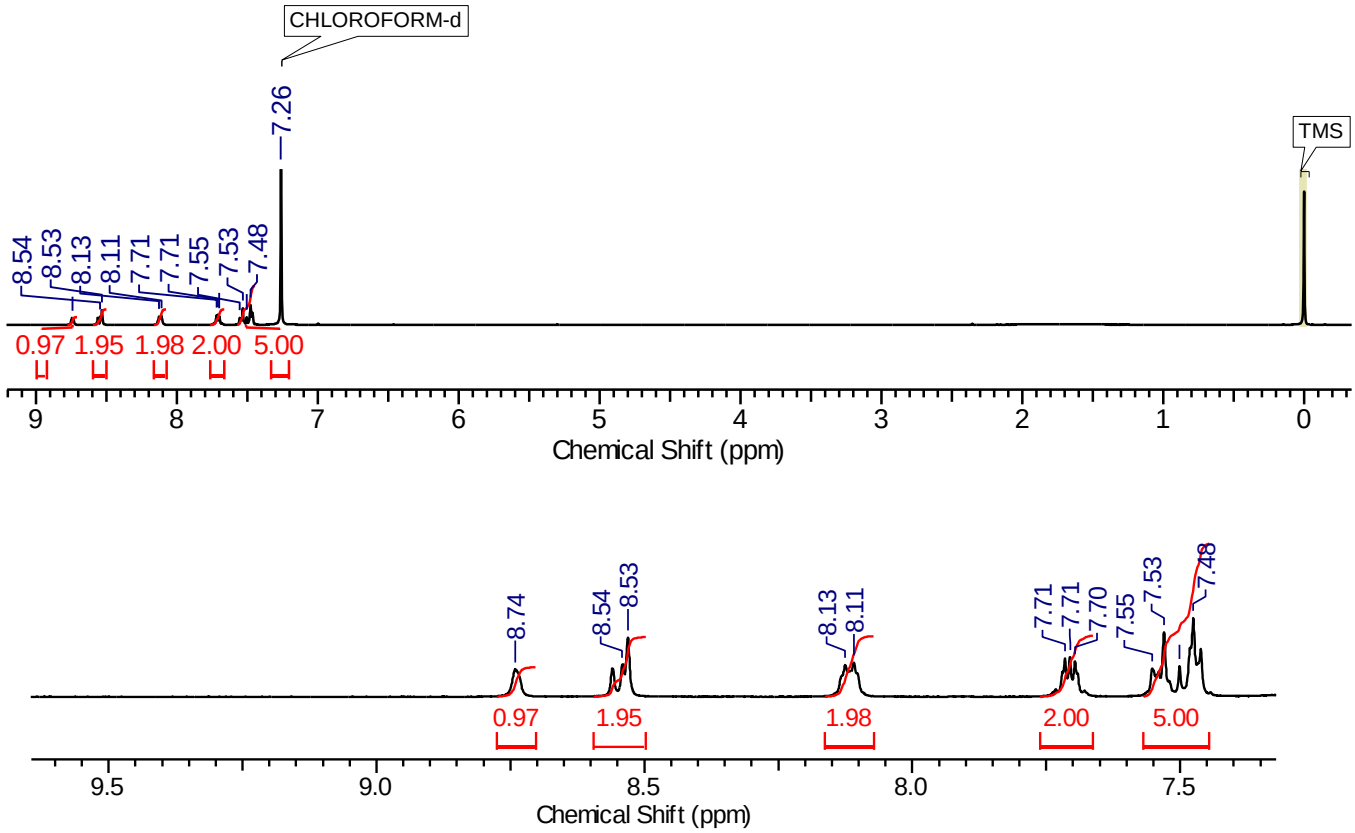

Fig. S5 ^{1}H NMR spectrum of **P2** ($CDCl_3$, 400 MHz).

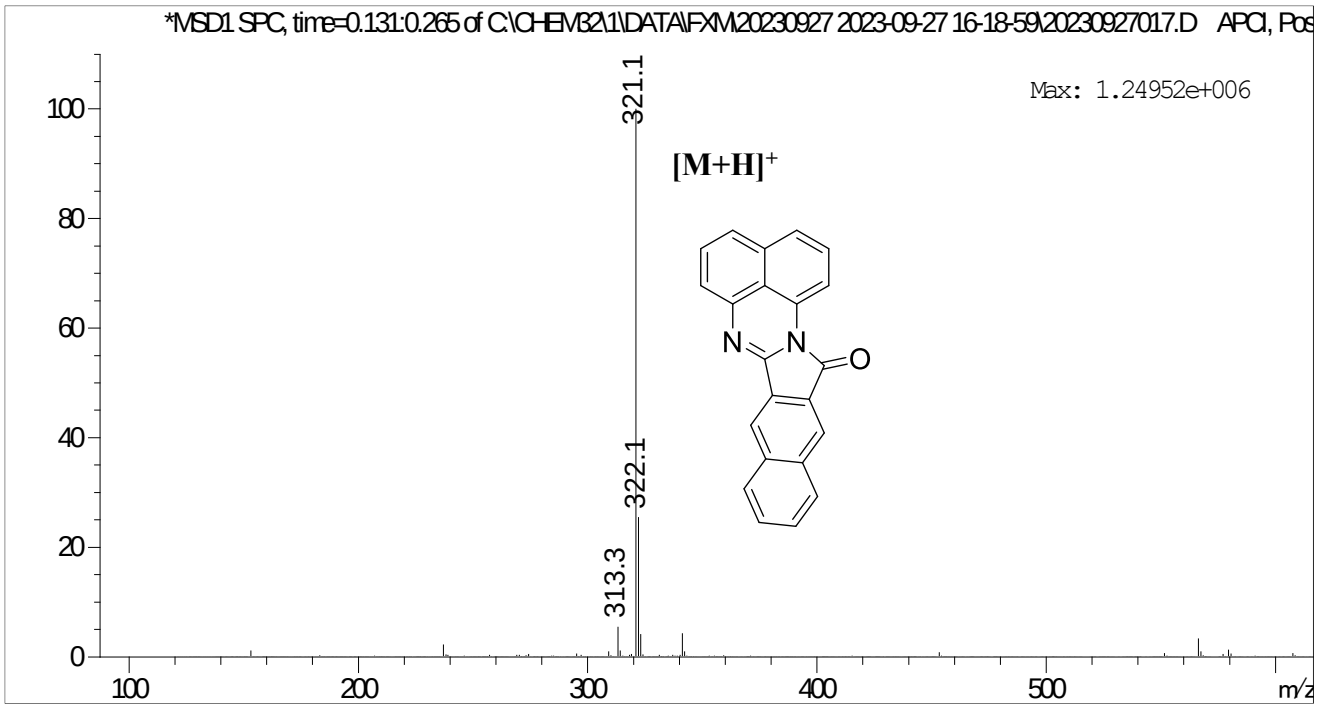

Fig. S6 APCI-MS of of **P2**.

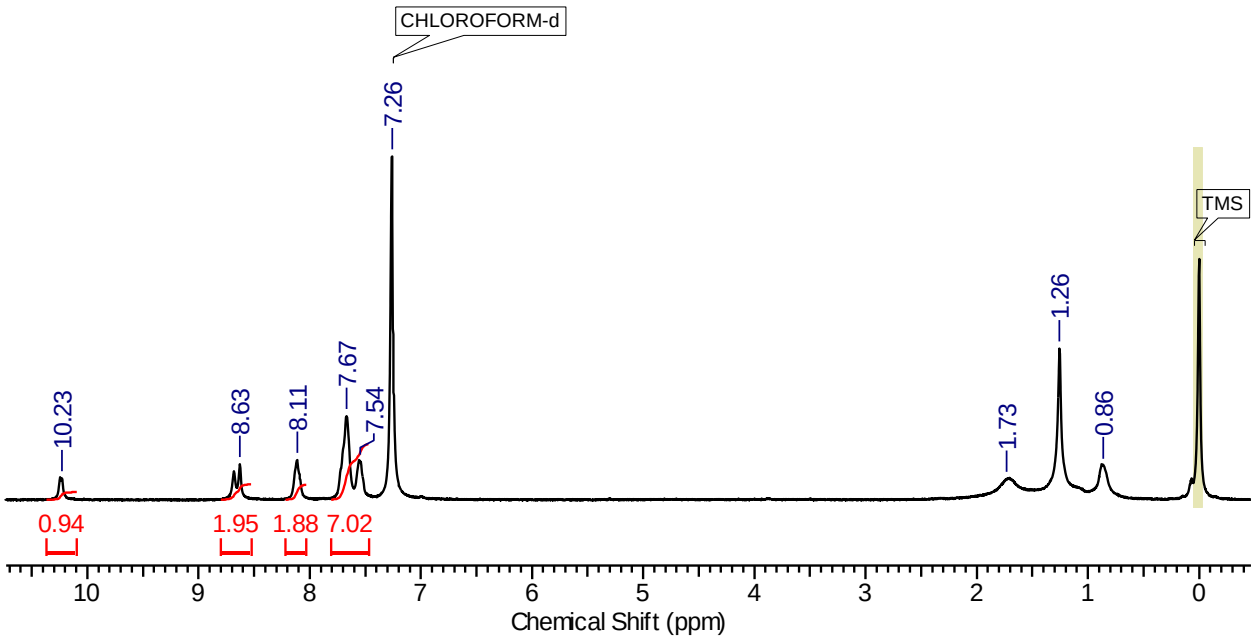

Fig. S7 ^{1}H NMR spectrum of **S2** ($CDCl_3$, 400 MHz).

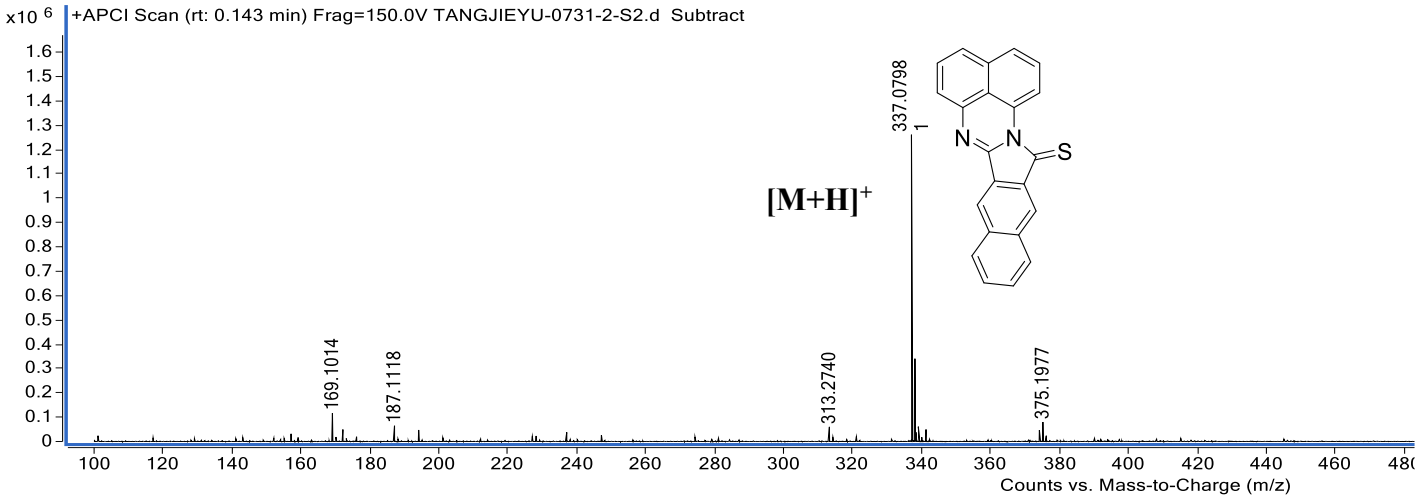

Fig. S8 APCI-MS of of **S2**.

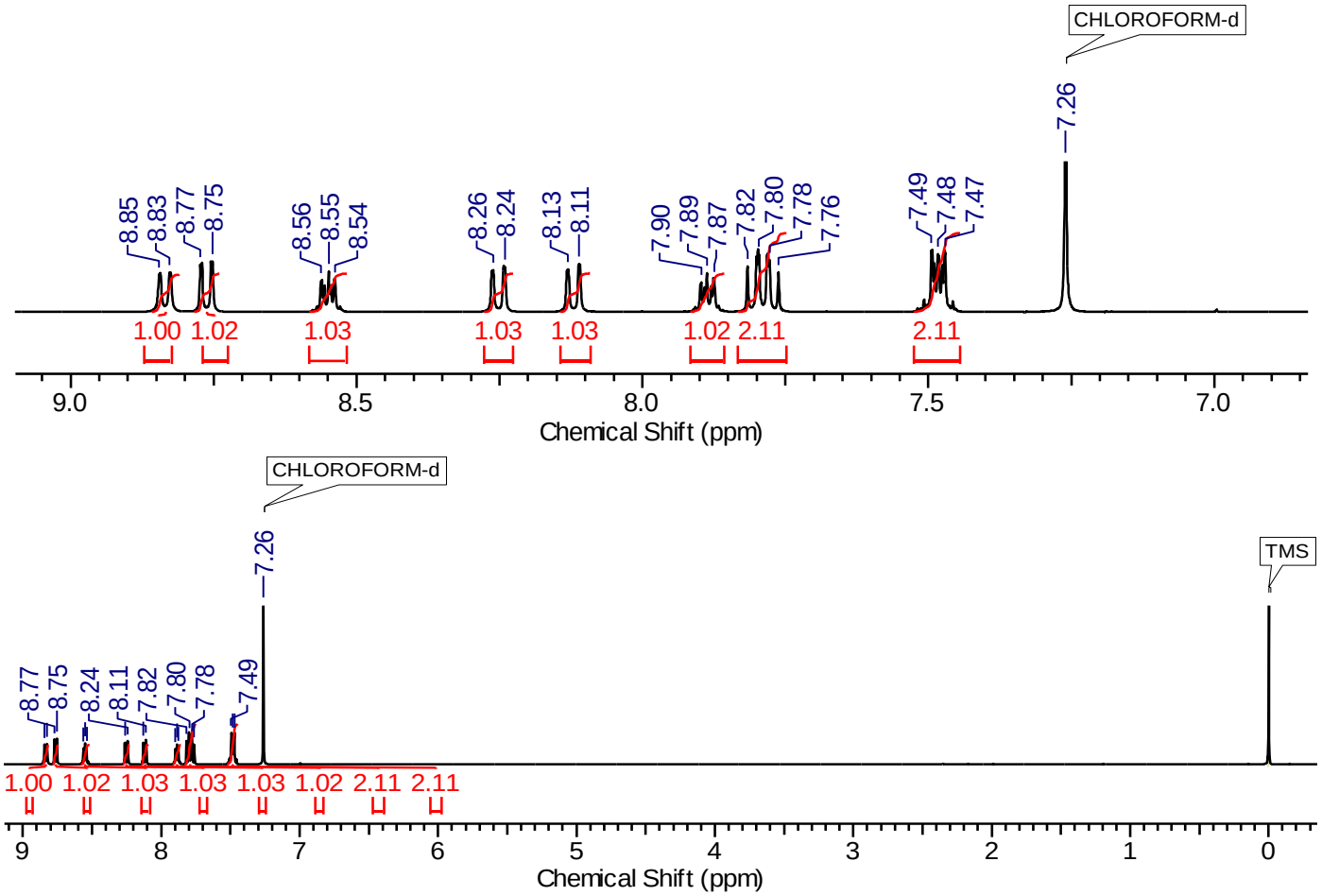

Fig. S9 ^{1}H NMR spectrum of **P3** ($CDCl_3$, 400 MHz).

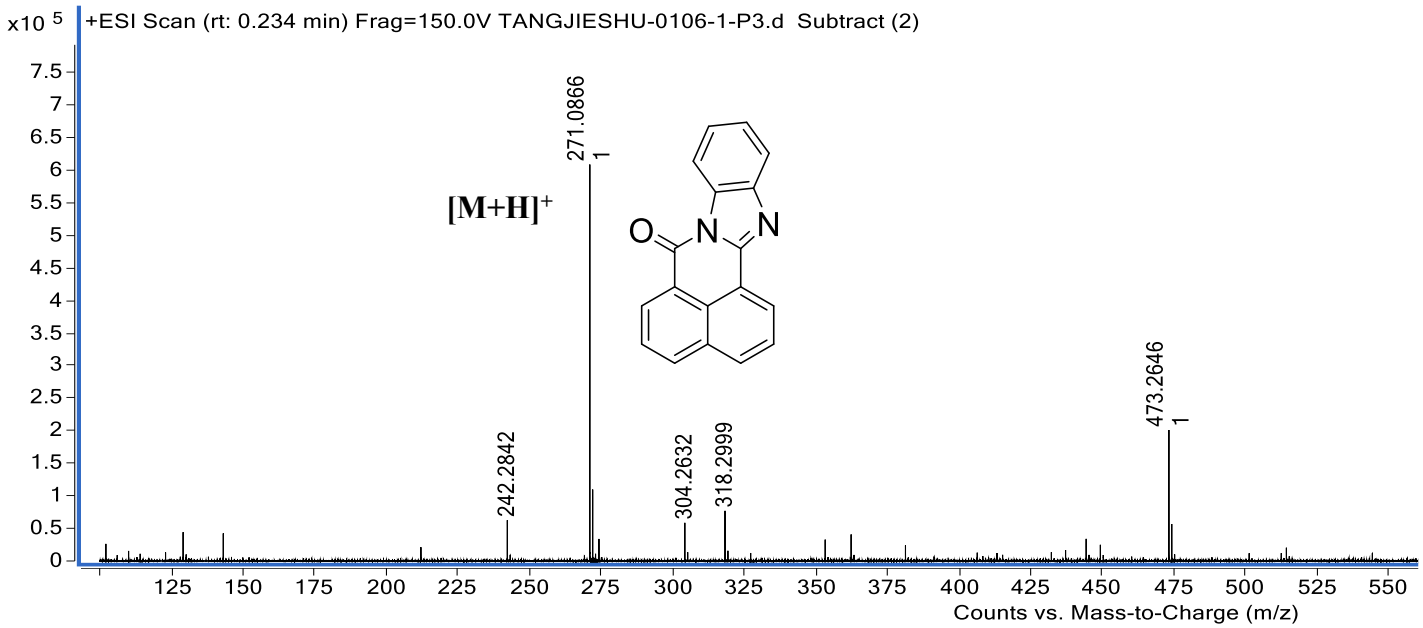

Fig. S10 APCI-MS of of **P3**.

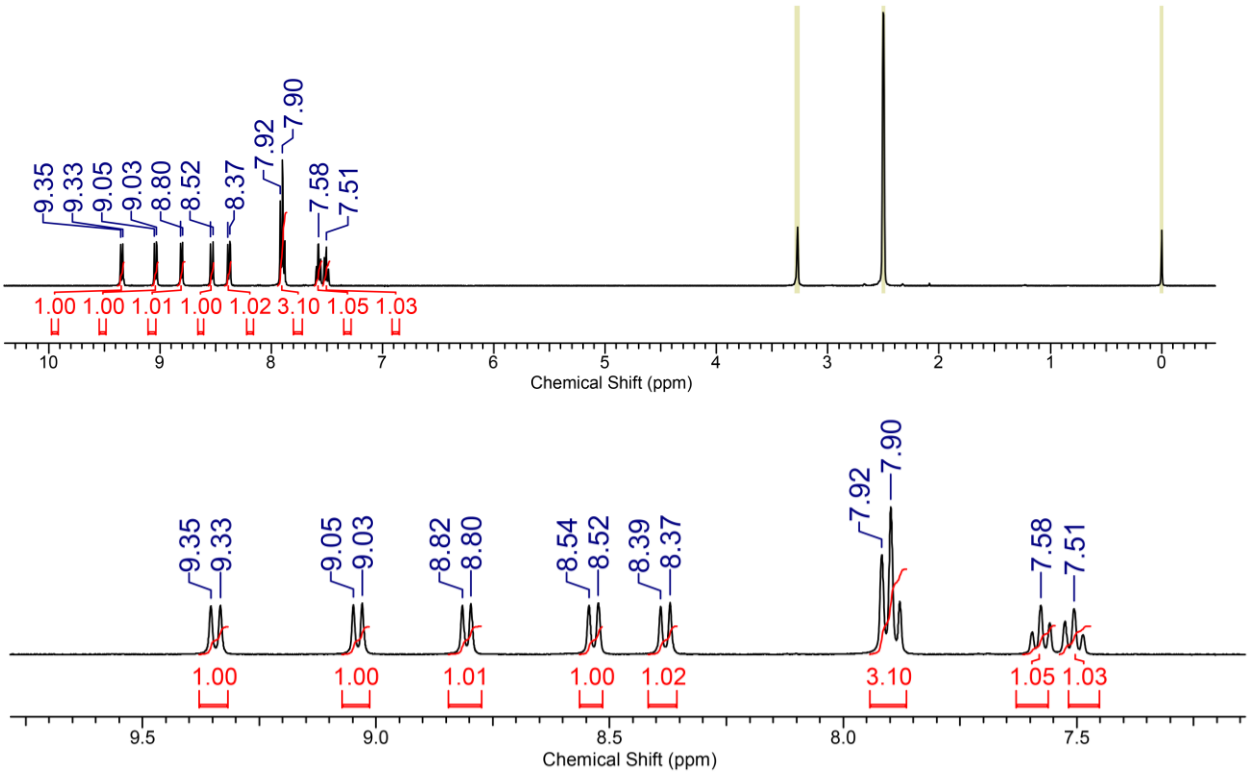

Fig. S11 ^{1}H NMR spectrum of **S3** (DMSO, 400 MHz).

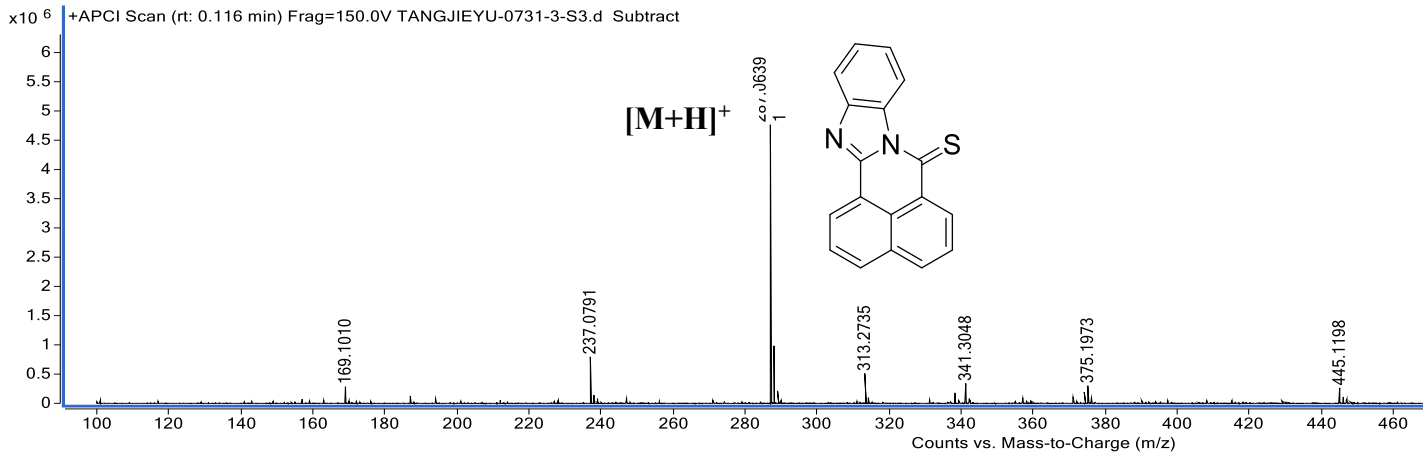

Fig. S12 APCI-MS of of **S3**.

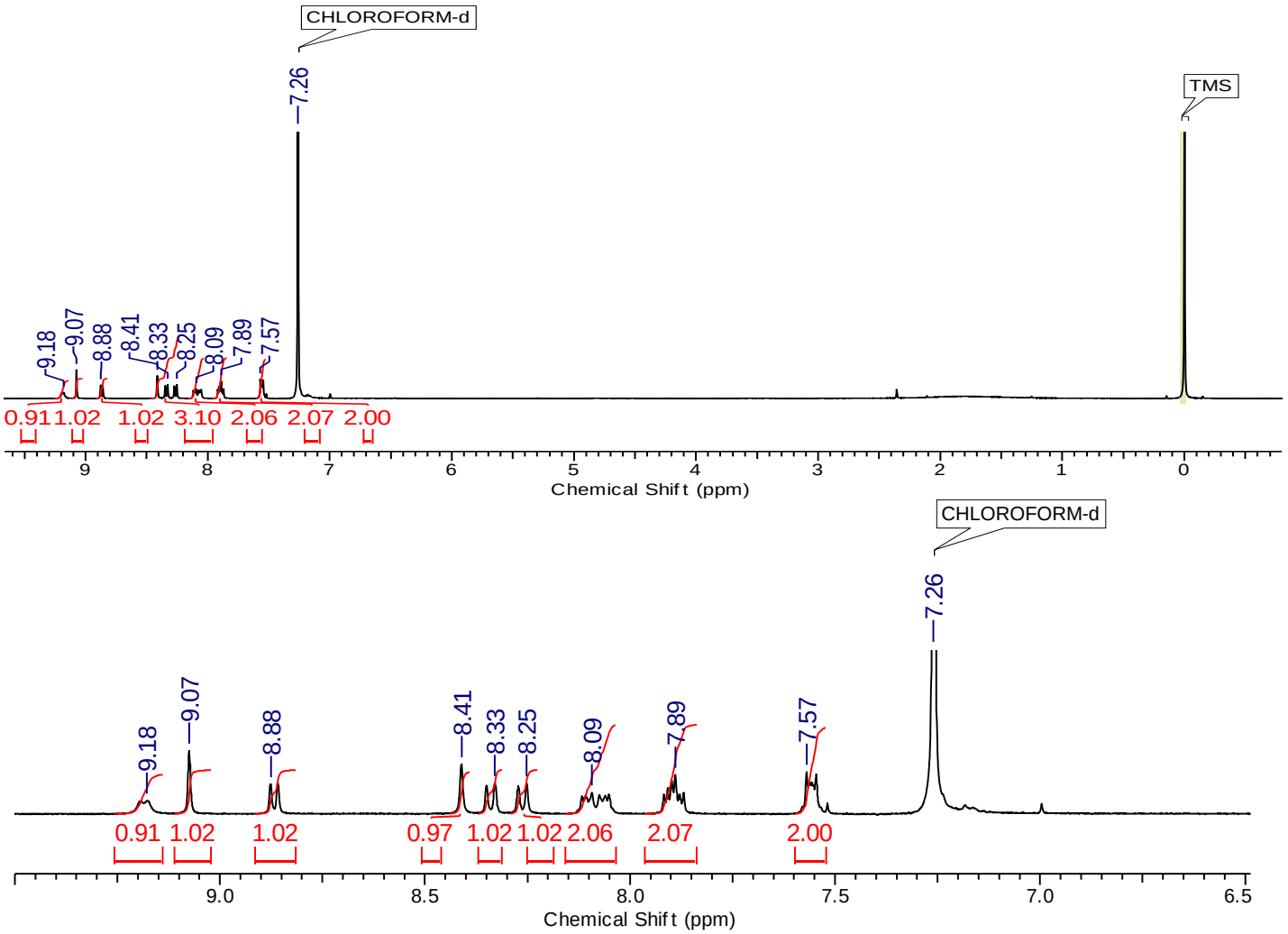

Fig. S13 ^{1}H NMR spectrum of **P4** ($CDCl_3$, 400 MHz).

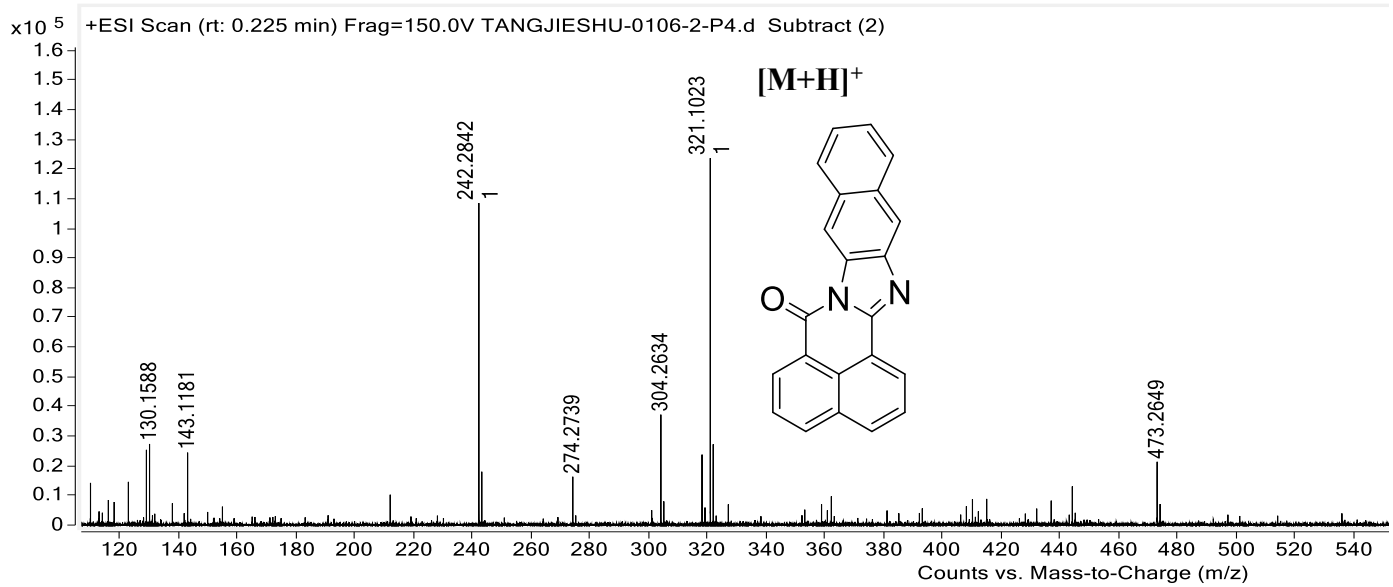

Fig. S14 ESI-MS of of **P4**.

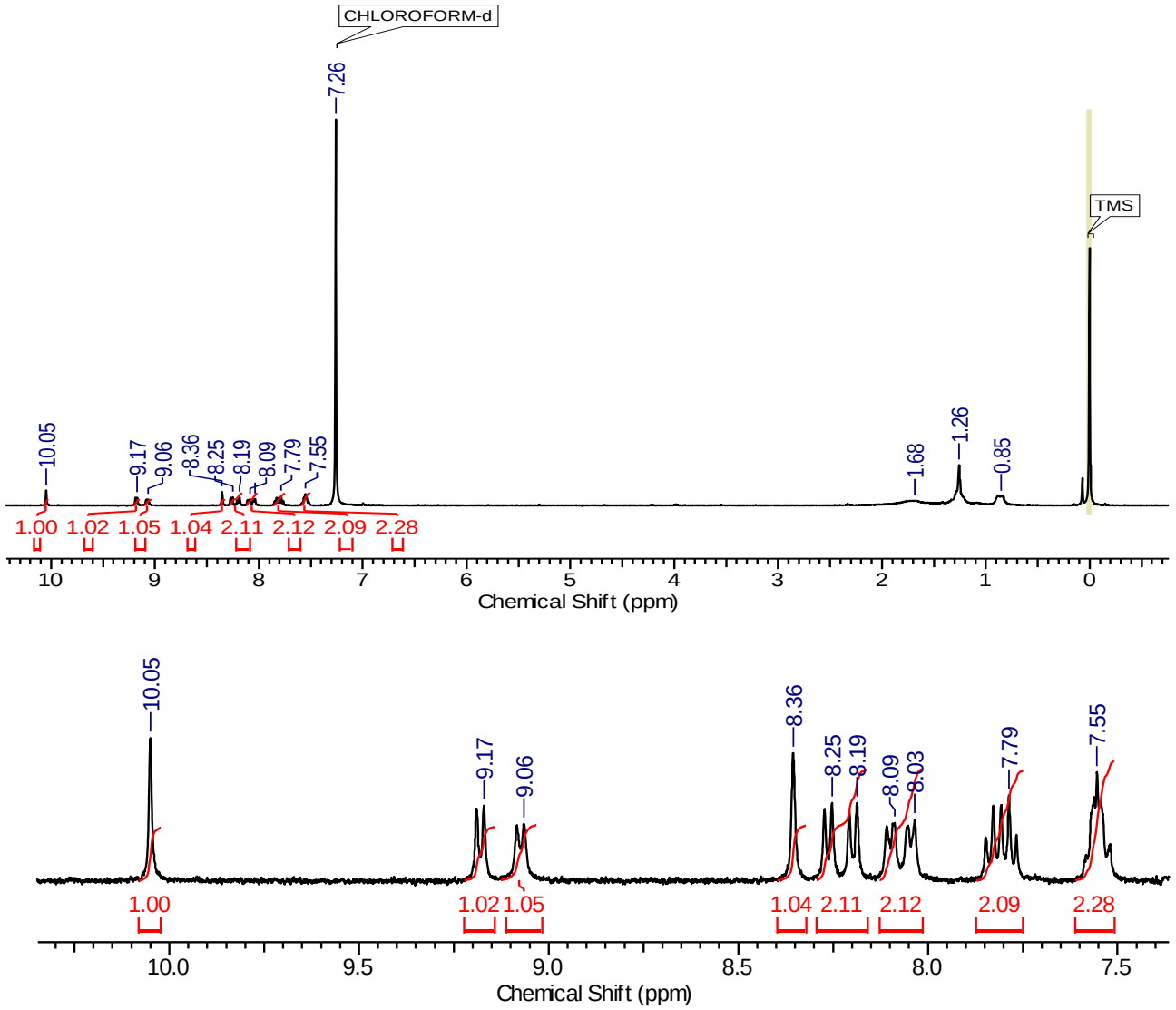

Fig. S15 ^{1}H NMR spectrum of **S4** ($CDCl_3$, 400 MHz).

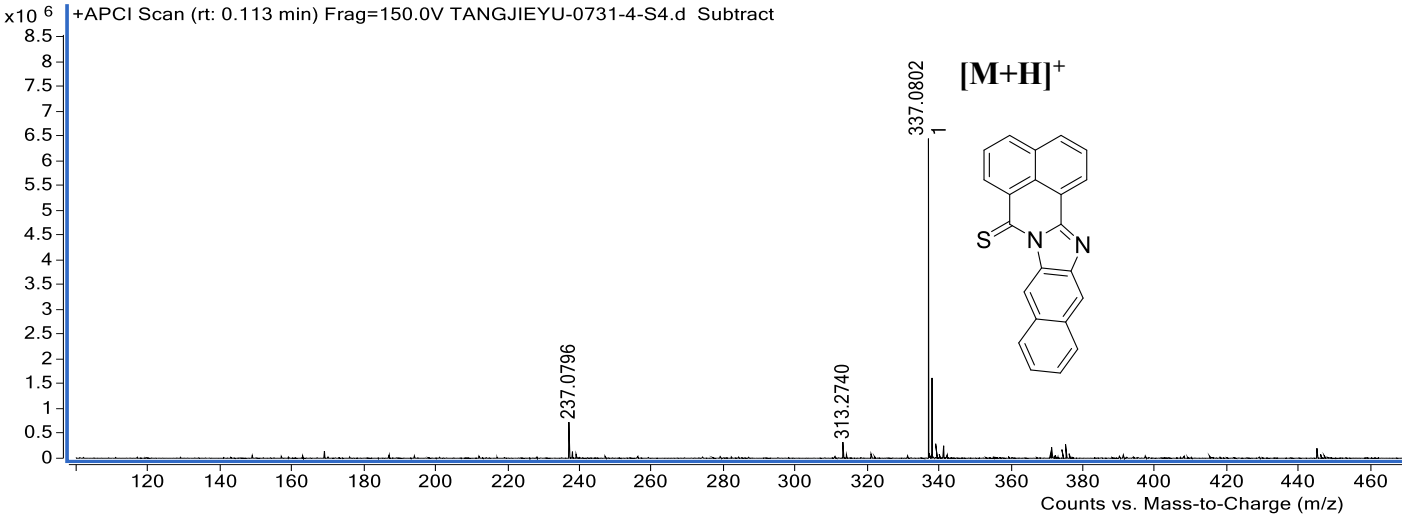

Fig. S16 APCI-MS of of **S4**.

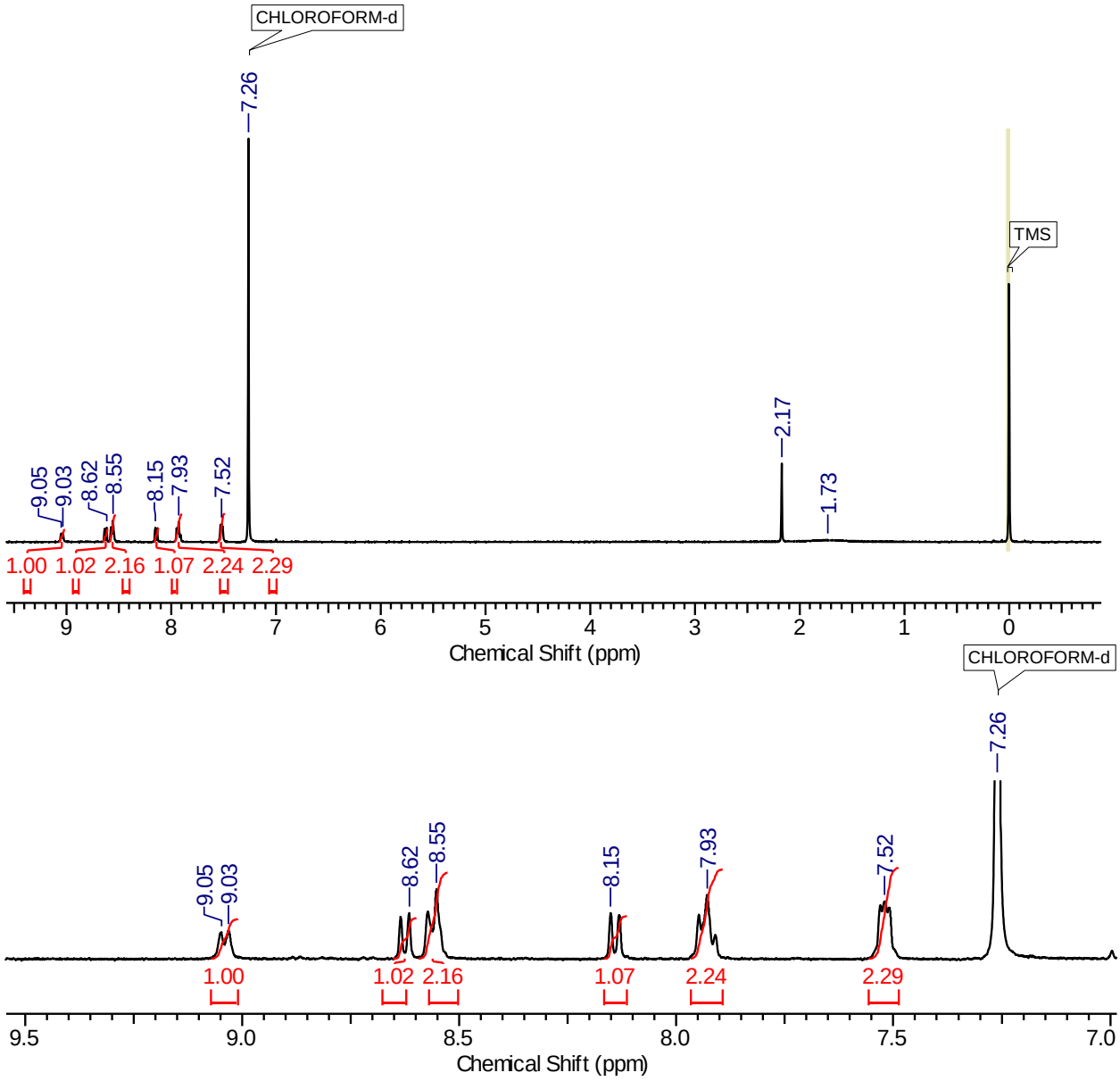

Fig. S17 ^{1}H NMR spectrum of **P3-Br** ($CDCl_3$, 400 MHz).

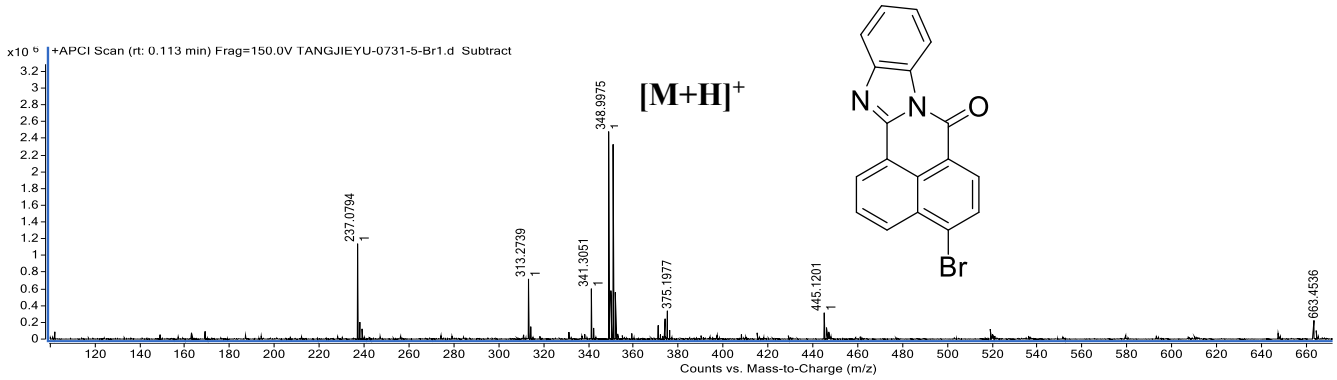

Fig. S18 APCI-MS of of **P3-Br**.

3. UV-vis Absorption and Fluorescence Emission Spectra

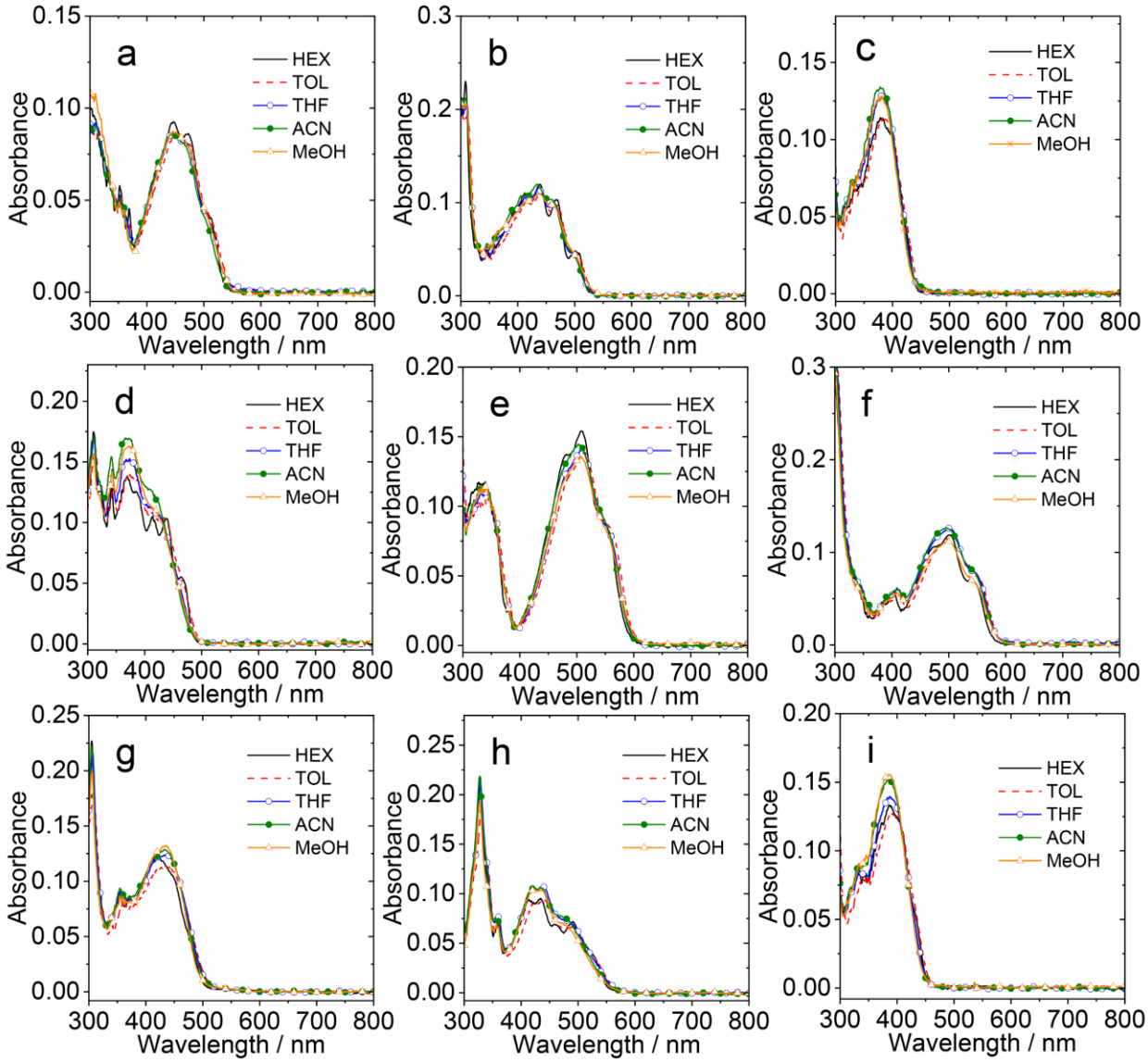

Fig. S19 UV-vis absorption spectra of (a) **P1**, (b) **P2**, (c) **P3**, (d) **P4**, (e) **S1**, (f) **S2**, (g) **S3**, (h) **S4** and (i) **P3-Br** in different polarity solvents. c= 1.0 ×10^{-5} M, 25 °C.

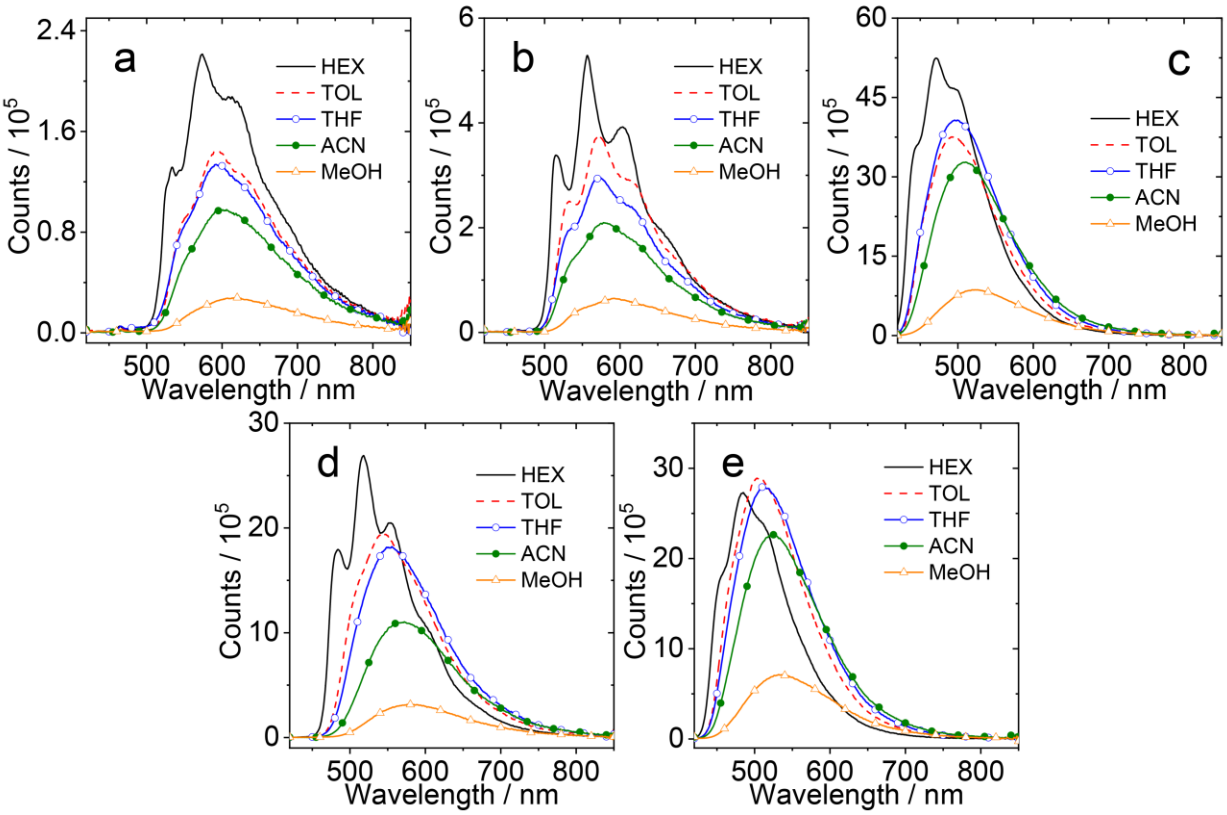

Fig. S20 Fluorescence spectra of (a) **P1**, (b) **P2**, (c) **P3**, (d) **P4** and (e) **P3-Br** in different polarity solvents. Optically matched solutions were used in each panel (each of the solutions gives the same absorbance at the excitation wavelength, A = 0.105), λ_{ex} = 410 nm, 25 °C.

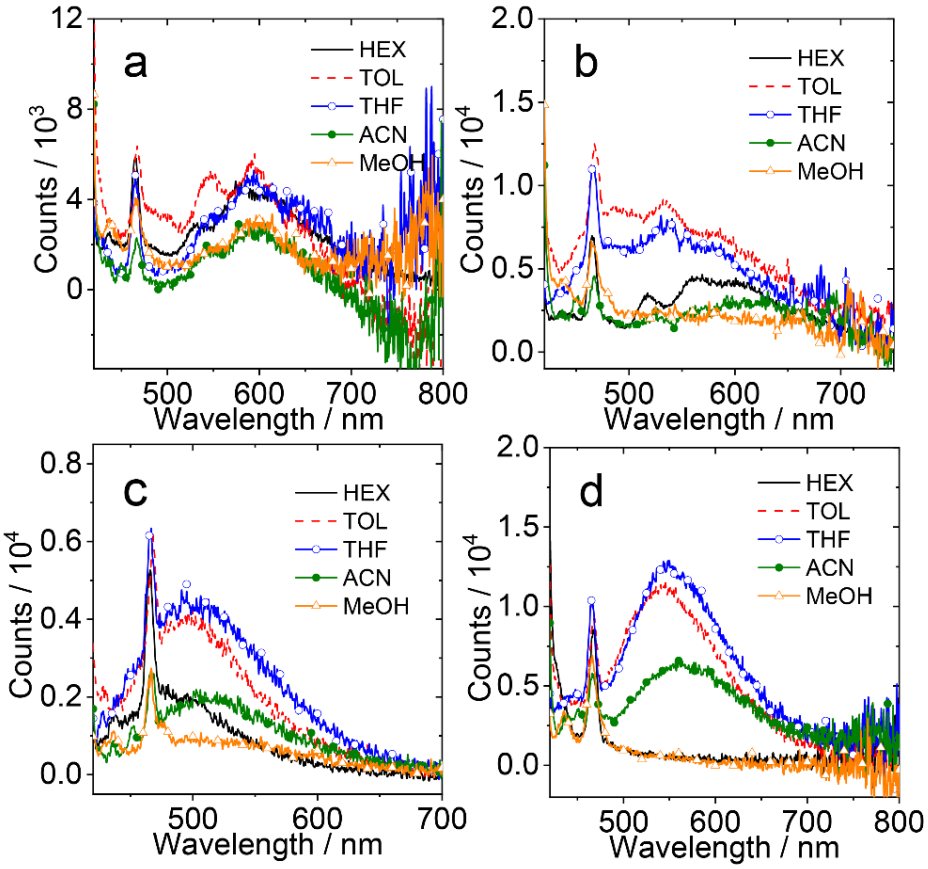

Fig. S21 Fluorescence spectra of (a) **S1**, (b) **S2**, (c) **S3** and (d) **S4** in different polarity solvents. Optically matched solutions were used in each panel (each of the solutions gives the same absorbance at the excitation wavelength, A = 0.105), λ_{ex} = 410 nm, 25 °C.

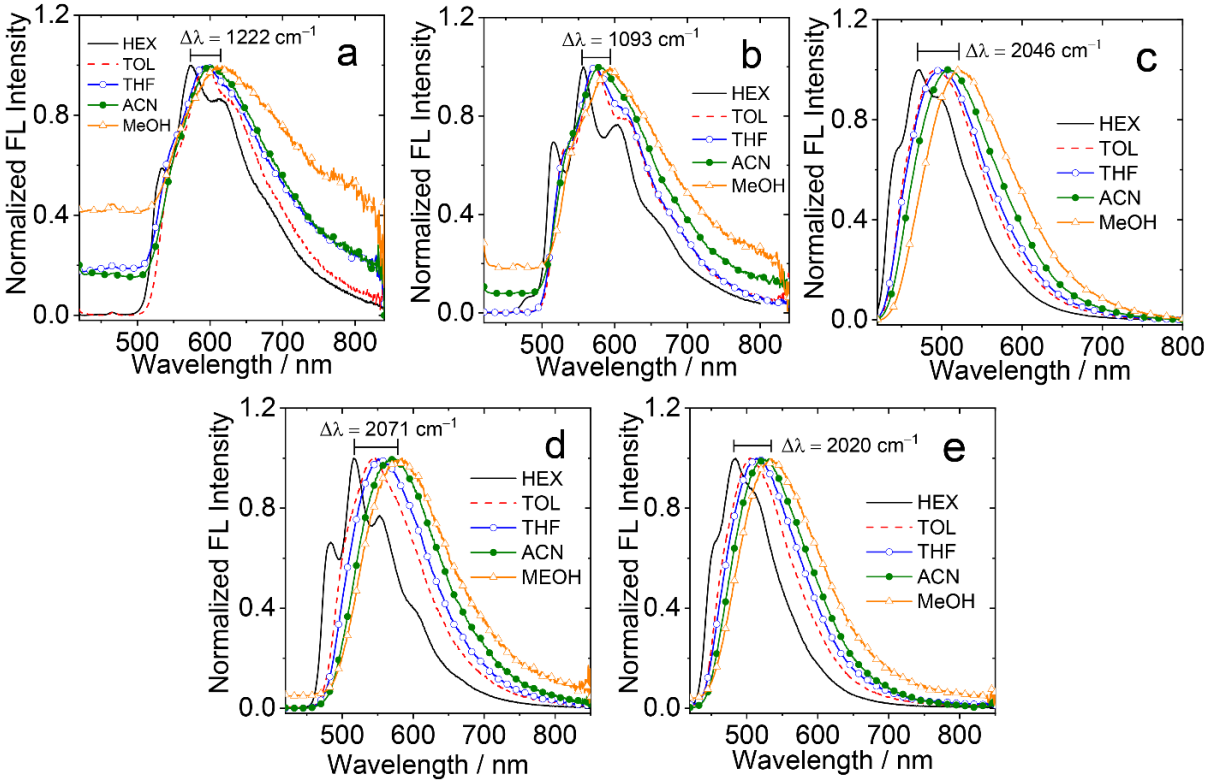

Fig. S22 Normalized fluorescence emission spectra of (a) **P1**, (b) **P2**, (c) **P3**, (d) **P4** and (e) **P3-Br** in different solvents.

4. Fluorescence Lifetime

Table S1. Fluorescence lifetimes of **P1**, **P2**, **P3**, **P4** and **P3-Br** in different solvent.[a]

Compound	HEX	TOL	THF	ACN	MeOH
P1	1.07 ns	0.84 ns	0.70 ns	0.54 ns	0.08 ns
P2	1.53 ns	1.34 ns	1.89 ns	0.90 ns	0.27 ns
P3	11.0 ns	10.6 ns	11.4 ns	11.8 ns	3.98 ns
P4	5.96 ns	6.55 ns	6.11 ns	4.35 ns	1.48 ns
P3-Br	5.16 ns	7.28 ns	8.38 ns	8.72 ns	8.00 ns

[a] Excited at 405 nm (Picosecond pulsed diode laser). c= 3.0 × 10^{-5} M in different solvent.

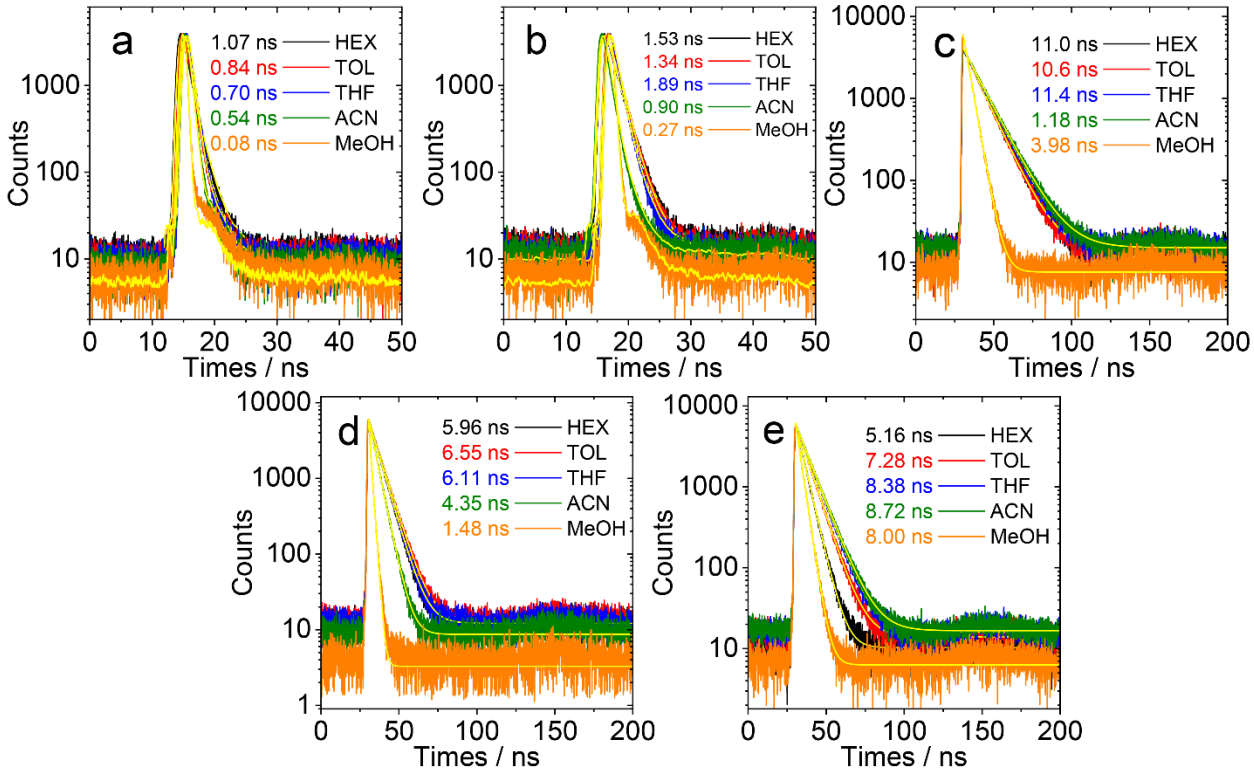

Fig. S23 Fluorescence decay trances of (a) **P1**, (b) **P2**, (c) **P3**, (d) **P4** and (e) **P3-Br** in different solvents. Excited with picosecond EPL laser (λ_{ex} = 405 nm), the fluorescence decay traces were monitored at (a) 570 nm, (b) 570 nm, (c) 470 nm, (d) 520 nm and (e) 480 nm, c = 3.0 × 10^{-5} M, 25 °C.

Table S2. Singlet Oxygen Quantum (Φ_Δ, in %) Yields and Absolute fluorescence Quantum (Φ_F, in %) Yields of Derivatives in Different Solvents.

	Quantum Yields	HEX[c]	TOL[d]	THF[e]	ACN[f]	MeOH[g]
P1[a]	Φ_F	5.4	4.9	4	2.8	1.1
	Φ_Δ	–[h]	0.5	0.3	0.2	0.2
S1[b]	Φ_F	0.5	0.4	0.4	0.2	0.2
	Φ_Δ	32	58	46	81	32
P2[a]	Φ_F	9.8	9.9	7.6	5.3	2.1
	Φ_Δ	–[h]	0.4	0.3	0.3	–[h]
S2[b]	Φ_F	0.3	0.3	0.3	0.3	0.2
	Φ_Δ	35	67	57	95	35
P3[a]	Φ_F	48.3	94.2	85.2	69.9	19.5
	Φ_Δ	–[h]	–[h]	–[h]	–[h]	23
S3[b]	Φ_F	0.3	0.5	0.5	0.4	0.3
	Φ_Δ	39	65	55	91	40
P4[a]	Φ_F	44.5	56.5	44.5	26.8	8.4
	Φ_Δ	–[h]	–[h]	–[h]	–[h]	22
S4[b]	Φ_F	0.2	0.4	0.5	0.2	0.3
	Φ_Δ	35	64	53	98	35
P3-Br[a]	Φ_F	43.8	65.9	61.6	50.5	16.7
	Φ_Δ	33	9	–[h]	8	7

[a] λ_{ex} = 410 nm. $Ru(bpy)_3[PF_6]_2$ was used as standard compound, Φ_Δ = 57% in DCM. [b] λ_{ex} = 490 nm. 2,6-didiiodoBodipy was used as standard compound, Φ_Δ = 87% in DCM. [c] HEX, $E_T(30)$ = 31.0 kcal/mol. [d] TOL, $E_T(30)$ = 33.9 kcal/mol. [e] Tetrahydrofuran, $E_T(30)$ = 37.4 kcal/mol. [f] ACN, $E_T(30)$ = 46.0 kcal/mol. [g] MeOH, $E_T(30)$ = 55.4 kcal/mol. [h] Not observed.

5. Electrochemical and Spectroelectrochemical Study

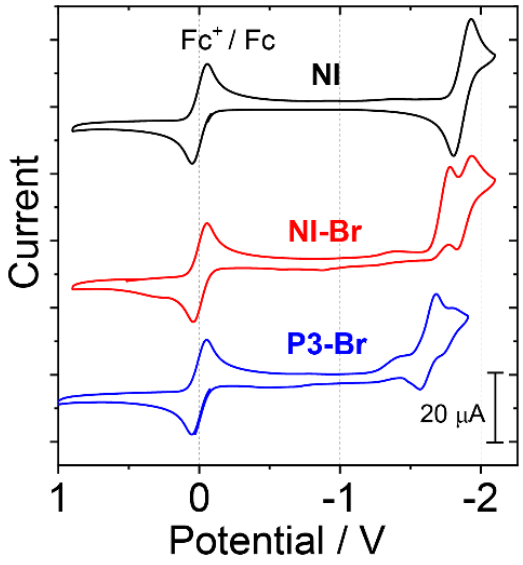

Fig. S24 Cyclic voltammograms of **NI**, **NI-Br** and **P3-Br** in deaerated DCM, 0.10 M Bu_4NPF_6 was used as the supporting electrolyte and $Ag/AgNO_3$ was used as the reference electrode. Scan rates: 100 mV s^{-1}. Ferrocene (Fc) was used as an internal reference.

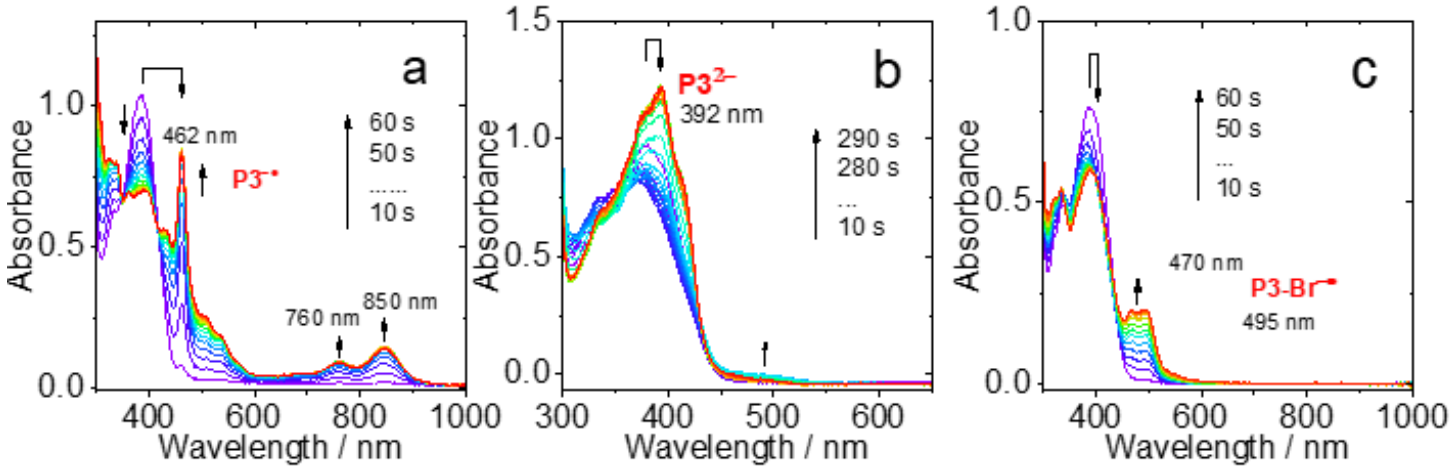

Fig. S25 Spectroelectrochemistry study of the dyad, i.e. the evolution of the UV-vis absorption of (a) **P3** upon oxidation with an applied potential of –1.77 V, (b) **P3** upon reduction with an applied potential of –2.36 V (c) **P3-Br** upon reduction with an applied potential of –1.63 V. The spectra were recorded in situ with a spectroelectrochemical cuvette (1 mm optical path). c = 1.0 × 10^{-4} M in deaerated DCM. 20 °C.

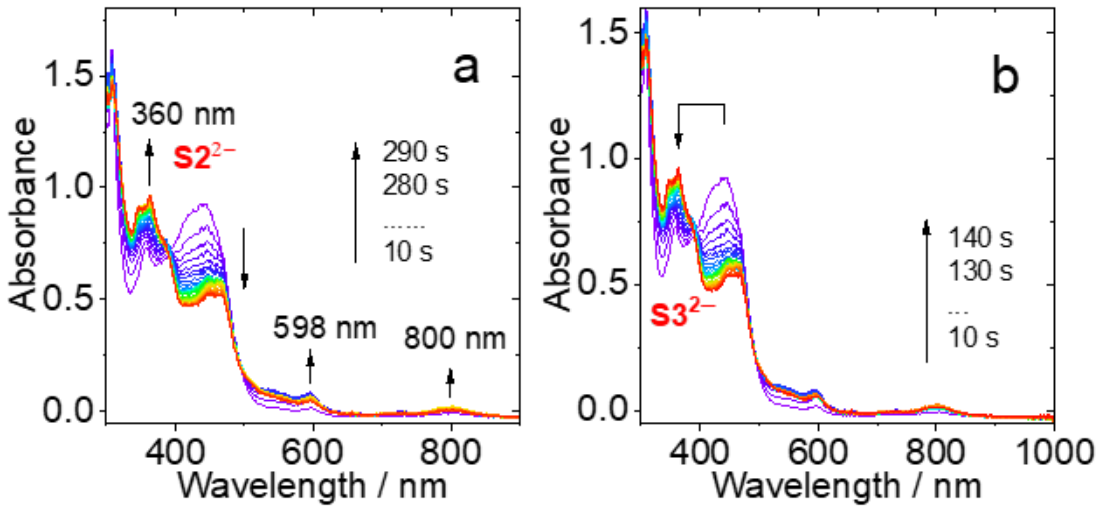

Fig. S26 Spectroelectrochemistry study of the dyad, i.e. the evolution of the UV-vis absorption of (a) **S2** and (b) **S3** upon reduction with an applied potential of –1.53 V. $Ag/AgNO_3$ was used as reference electrode. The spectra were recorded in situ with a spectroelectrochemical cuvette (1 mm optical path). c = 6.0 × 10^{-5} M in deaerated DCM. 20 °C.

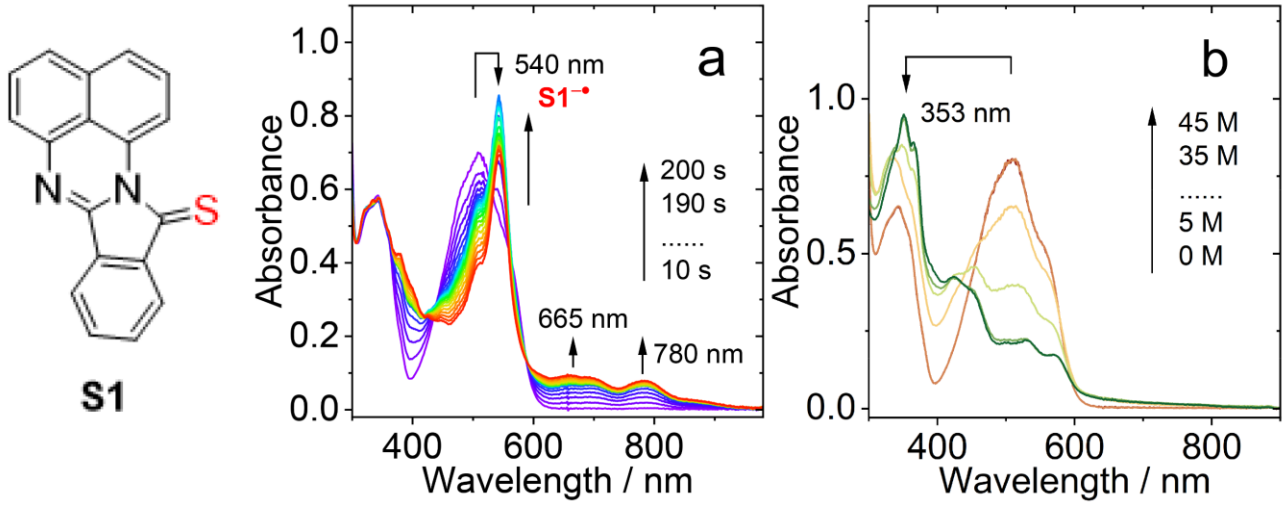

Fig. S27 (a) Spectroelectrochemistry study of the dyad, i.e. the evolution of the UV-vis absorption of **S1** upon reduction with an applied potential of –1.39 V. $Ag/AgNO_3$ was used as reference electrode. The spectra were recorded in situ with a spectroelectrochemical cuvette (1 mm optical path). c = 6.0 × 10^{-5} M in deaerated DCM. 20 °C. (b) UV-vis absorption spectra of **S1** chemically reduced with TBAF used to generate **S1**$^{-\bullet}$ in deaerated DMF. c = 1.0 × 10^{-4} M. 20 °C.

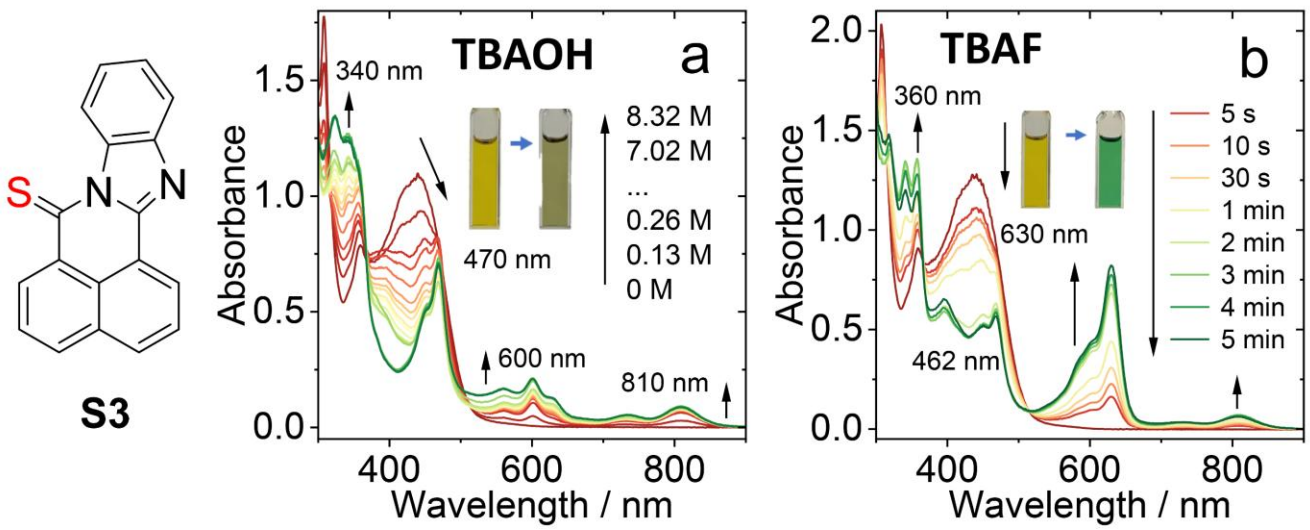

Fig. S28 UV-vis absorption spectra of **S3** chemically reduced with (a) tetrabutylammonium hydroxide (TBAOH) and (b) tetrabutylammonium fluoride (TBAF) used to generate $S3^{-\bullet}$ in deaerated DMF. c = 1.0 × 10^{-4} M. 20 °C.

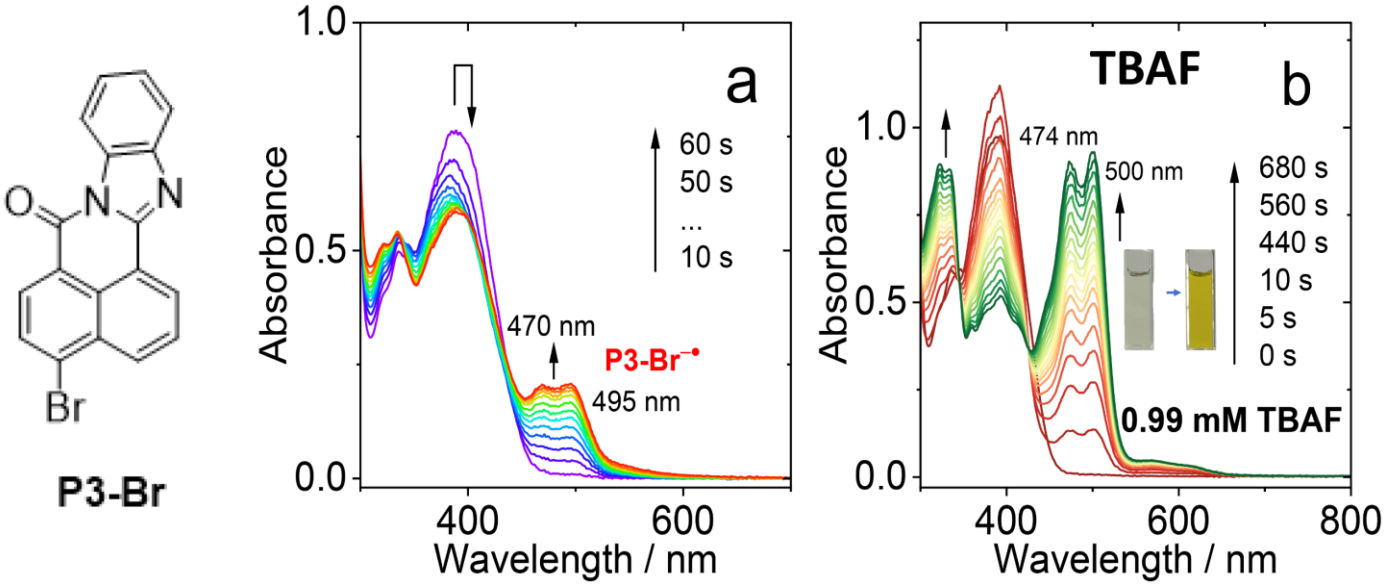

Fig. S29 (a) **P3-Br** upon reduction with an applied potential of –1.63 V. The spectra were recorded in situ with a spectroelectrochemical cuvette (1 mm optical path), in deaerated DCM. (b) UV-vis absorption spectra of **P3-Br** chemically reduced with TBAF used to generate **P3-Br**$^{-\bullet}$ in deaerated DMF. c = 1.0 × 10^{-4} M. 20 °C.

6. Femtosecond Transient Absorption Spectra

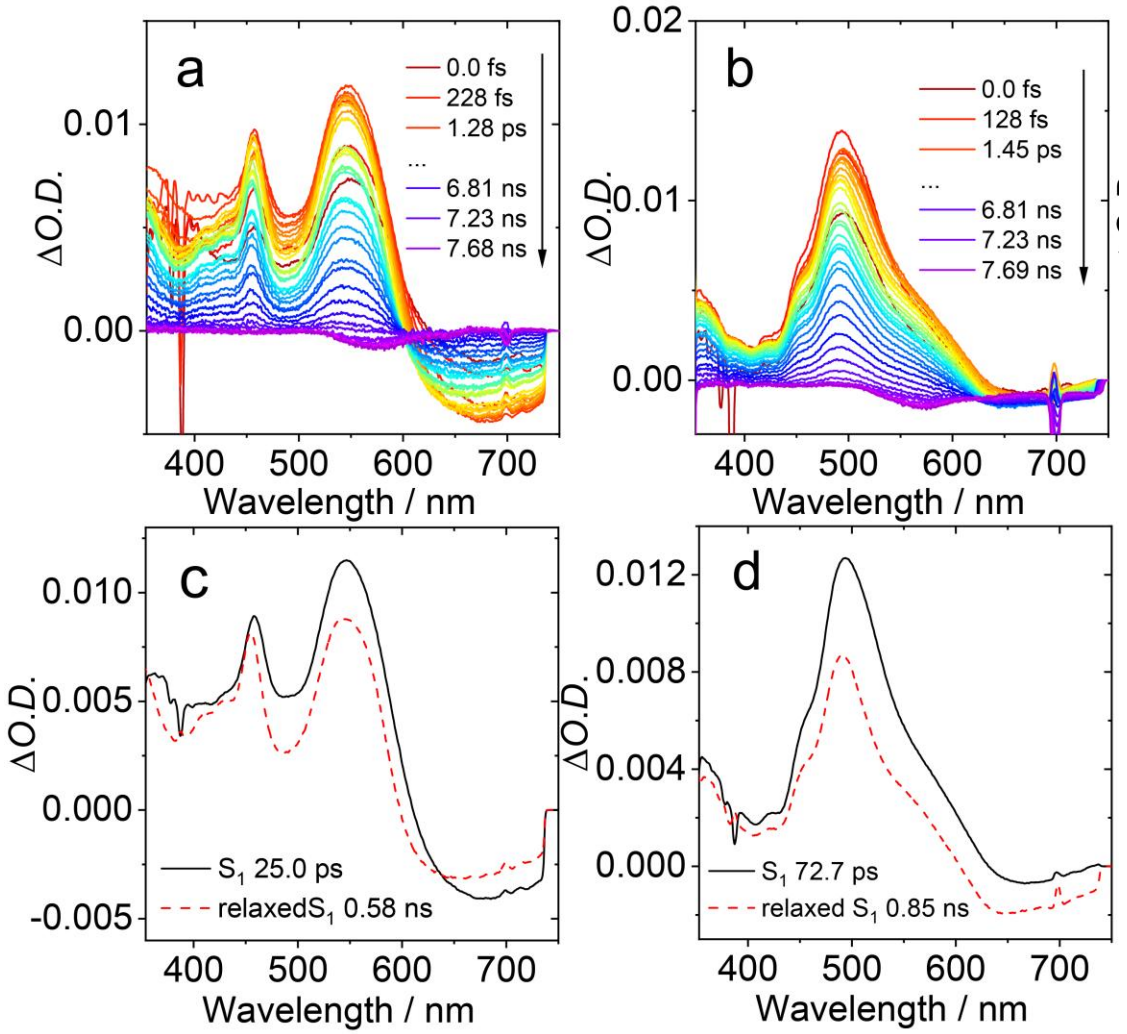

Fig. S30 Femtosecond transient absorption spectra of (a) **P1** and (b) **P2** in ACN, and relative EADS of (c) **P1** and (d) **P2** obtained from target analysis with the sequential model. The raw data are reported in (a) and (b). Excited at 350 nm.

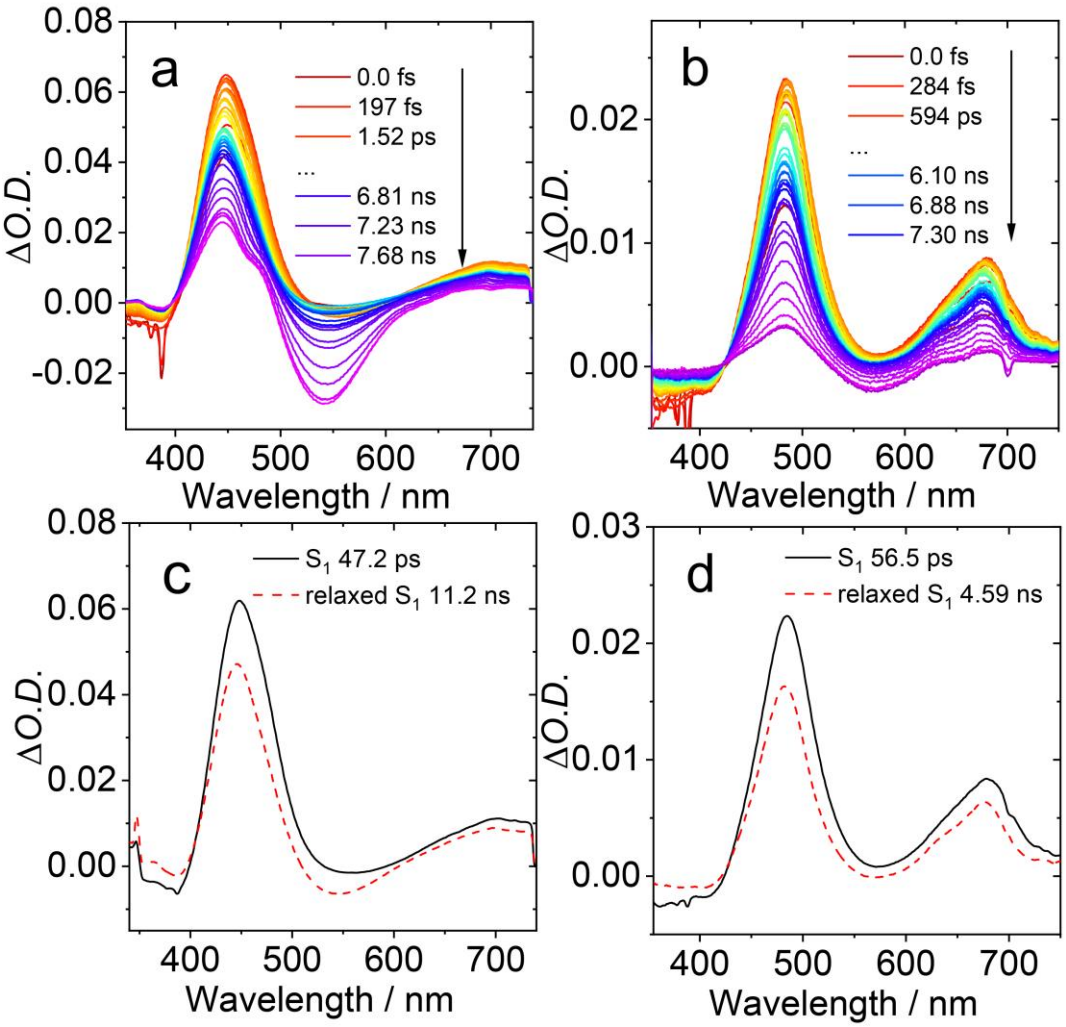

Fig. S31 Femtosecond transient absorption spectra of (a) **P3** and (b) **P4** in ACN, and relative EADS of (c) **P3** and (d) **P4** obtained from target analysis with the sequential model. The raw data are reported in (a) and (b). Excited at 350 nm.

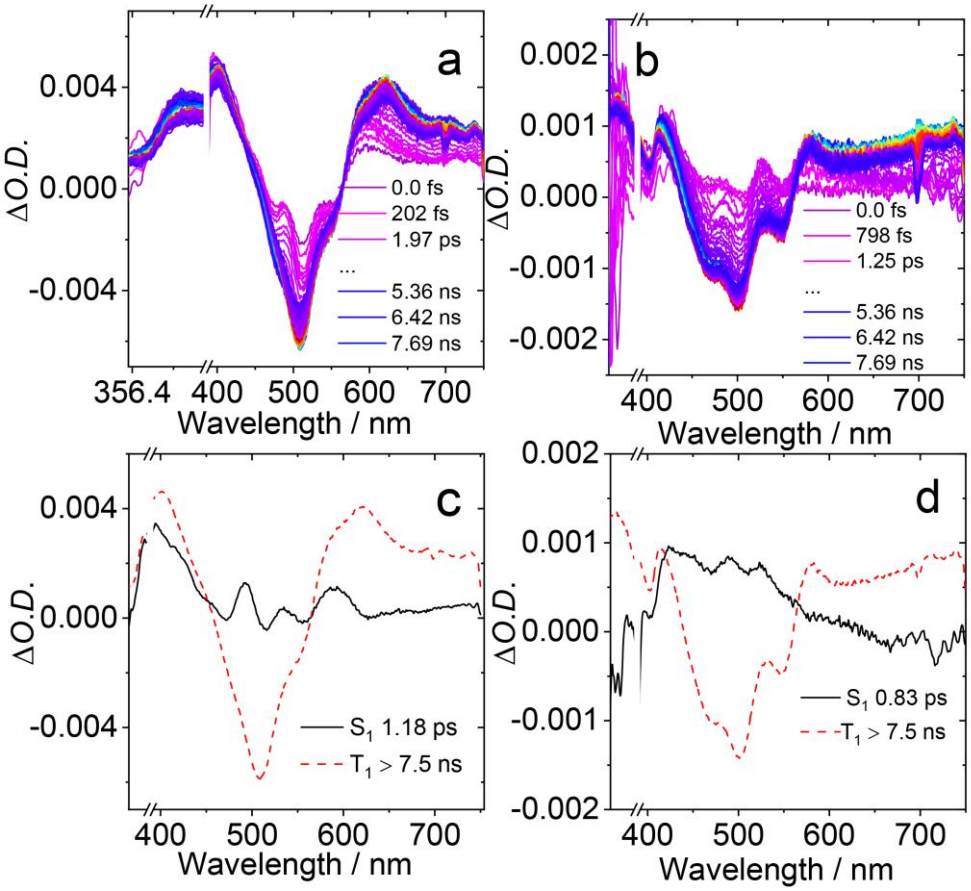

Fig. S32 Femtosecond transient absorption spectra of (a) **S1** and (b) **S2** in HEX, and relative EADS of (c) **S1** and (d) **S2** obtained from target analysis with the sequential model. The raw data are reported in (a) and (b). Excited at 350 nm.

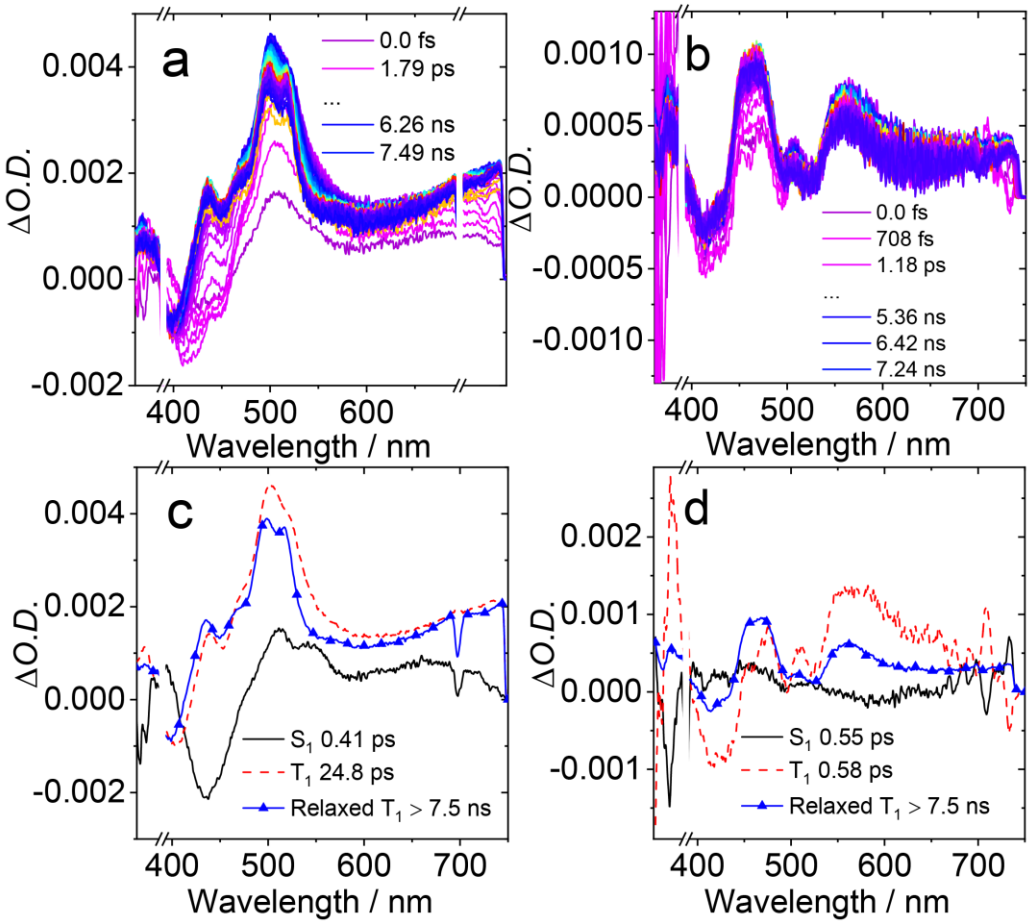

Fig. S33 Femtosecond transient absorption spectra of (a) **S3** and (b) **S4** in ACN, and relative EADS of (c) **S3** and (d) **S4** obtained from target analysis with the sequential model. The raw data are reported in (a) and (b). Excited at 350 nm.

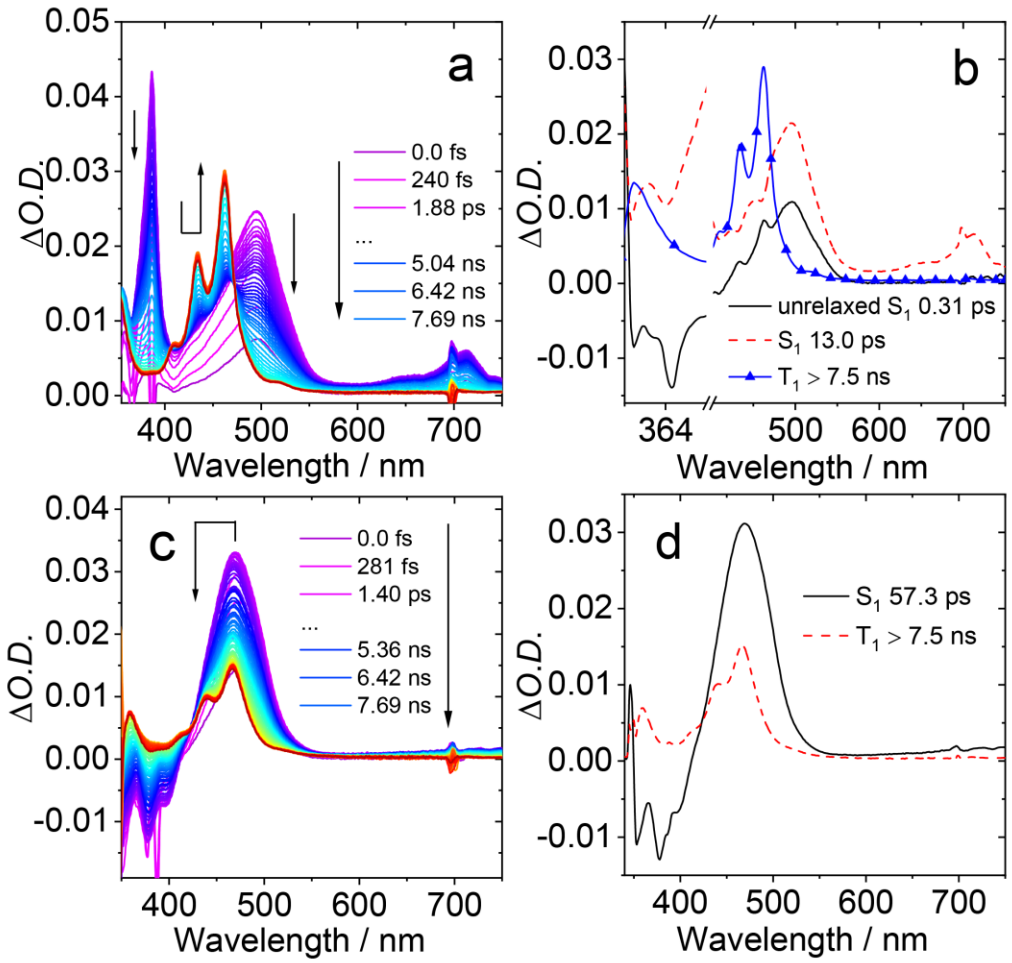

Fig. S34 Femtosecond transient absorption spectra of **NI** with excitation at 350 nm in (a) HEX and (c) ACN, (b) and (d) are corresponding evolution associated difference spectra (EADS) of (a) and (c), respectively, obtained by target analysis.

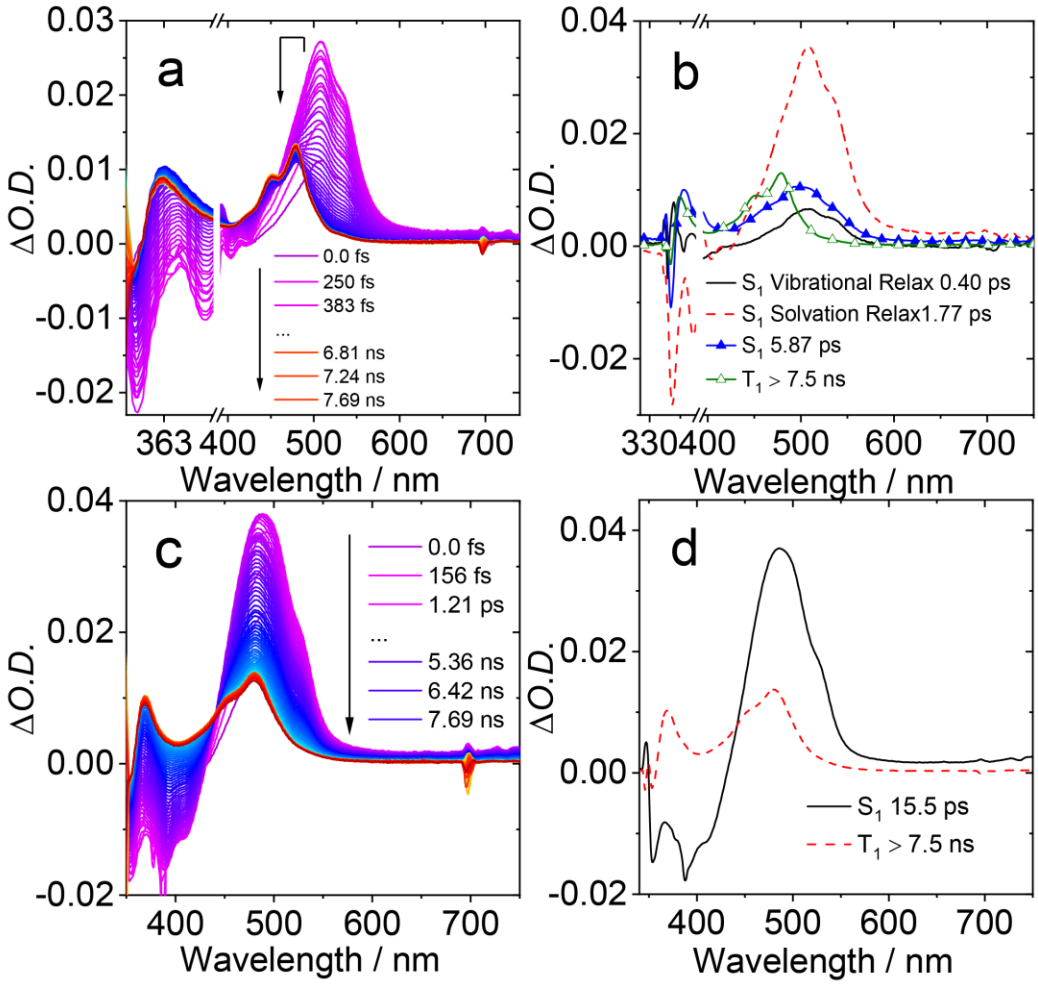

Fig. S35 Femtosecond transient absorption spectra of **NI-Br** with excitation at 350 nm in (a) HEX and (c) ACN, (b) and (d) are corresponding evolution associated difference spectra (EADS) of (a) and (c), respectively, obtained by target analysis.

7. Nanosecond Transient Absorption Spectra

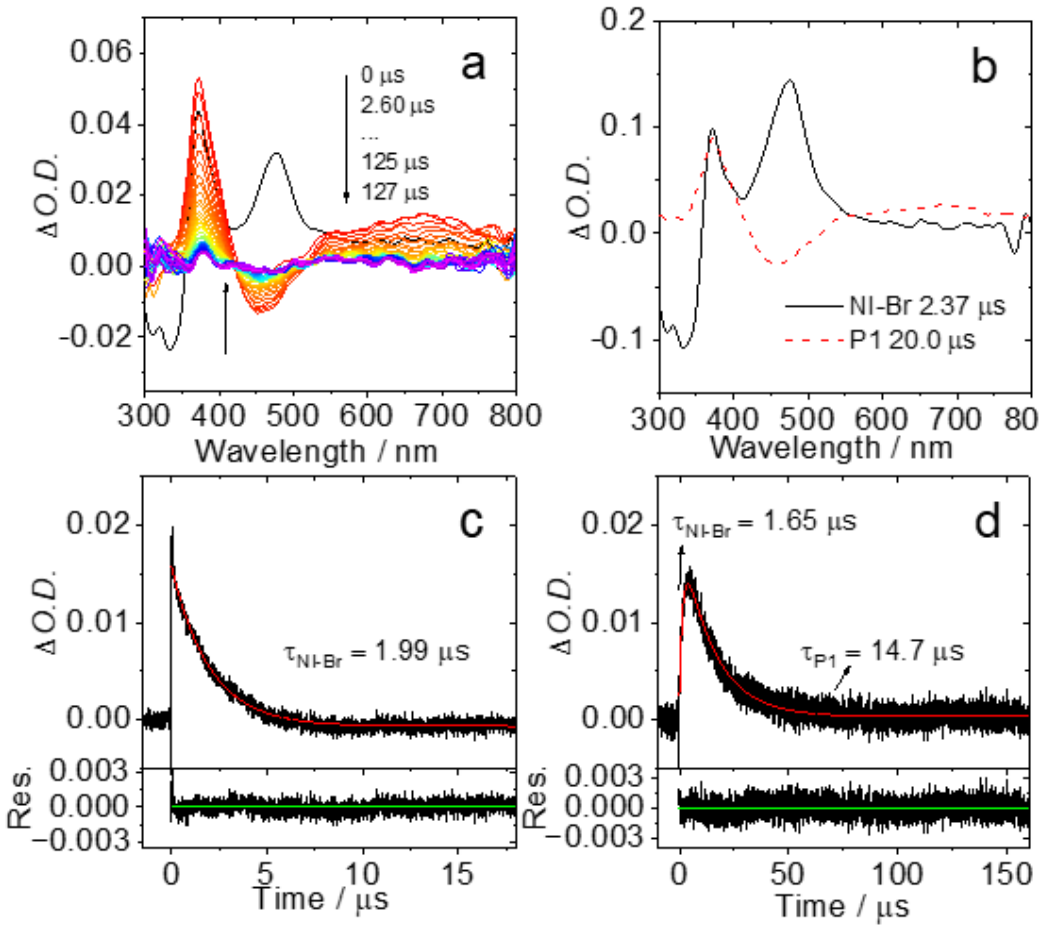

Fig. S36 (a) Intermolecular triplet energy transfer with **NI-Br** as the triplet energy donor and **P1** as the triplet energy acceptor, studied with nanosecond transient absorption spectra. *c* [**P1**] = 2.5 x 10^{-5}M, *c* [**NI-Br**] = 1.0 x 10^{-5}M, λ_{ex} = 355 nm, in deaerated acetonitrile, 25 °C.(b) Species-associated difference spectra (SADS) of the mixture of **NI-Br** with **P1**. The raw data are from (a). Analyzed with global fitting and target analysis. (c) the decay trace at 510 nm. (d) the decay trace at 670 nm.

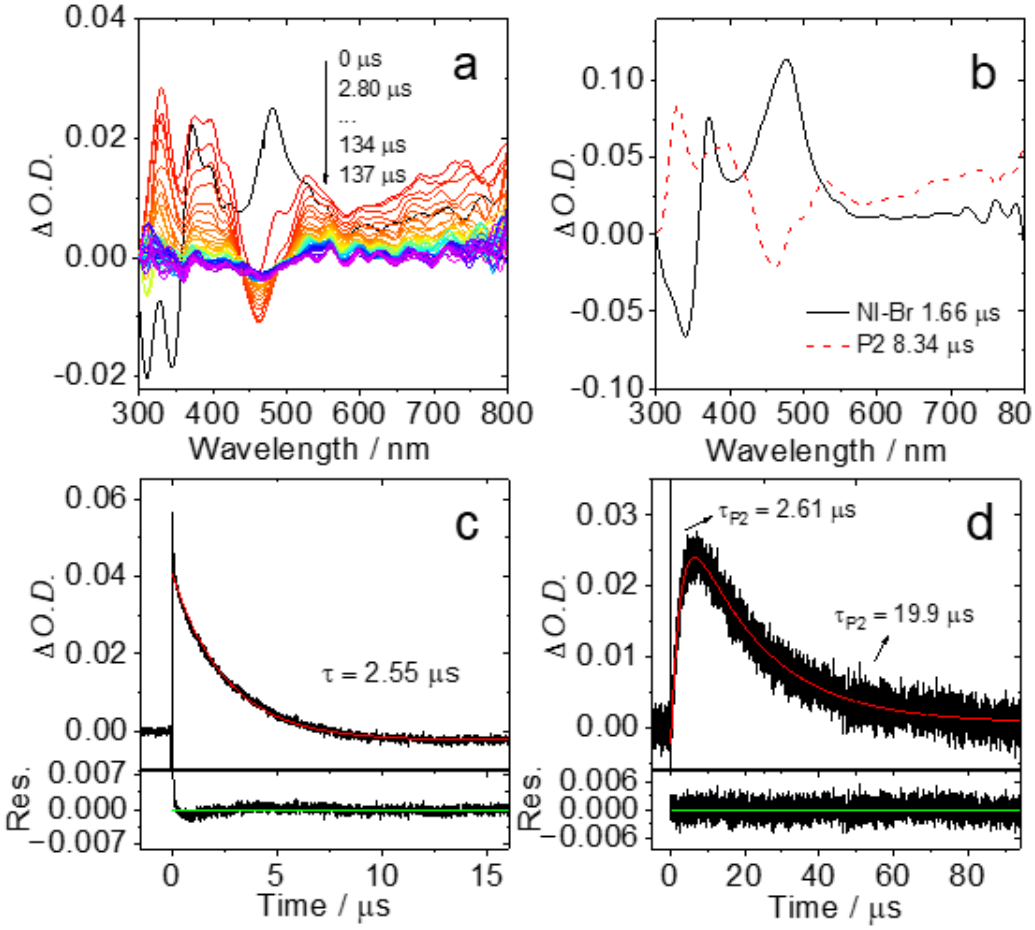

Fig. S37 (a) Intermolecular triplet energy transfer with **NI-Br** as the triplet energy donor and **P1** as the triplet energy acceptor, studied with nanosecond transient absorption spectra. *c* [**P2**] = 2.5 x 10^{-5}M, *c* [**NI-Br**] = 1.0 x 10^{-5}M, λ_{ex} = 355 nm, in deaerated acetonitrile, 25 °C.(b) Species-associated difference spectra (SADS) of the mixture of **NI-Br** with **P2**. The raw data are from (a). Analyzed with global fitting and target analysis. (c) the decay trace at 490 nm. (d) the decay trace at 330 nm.

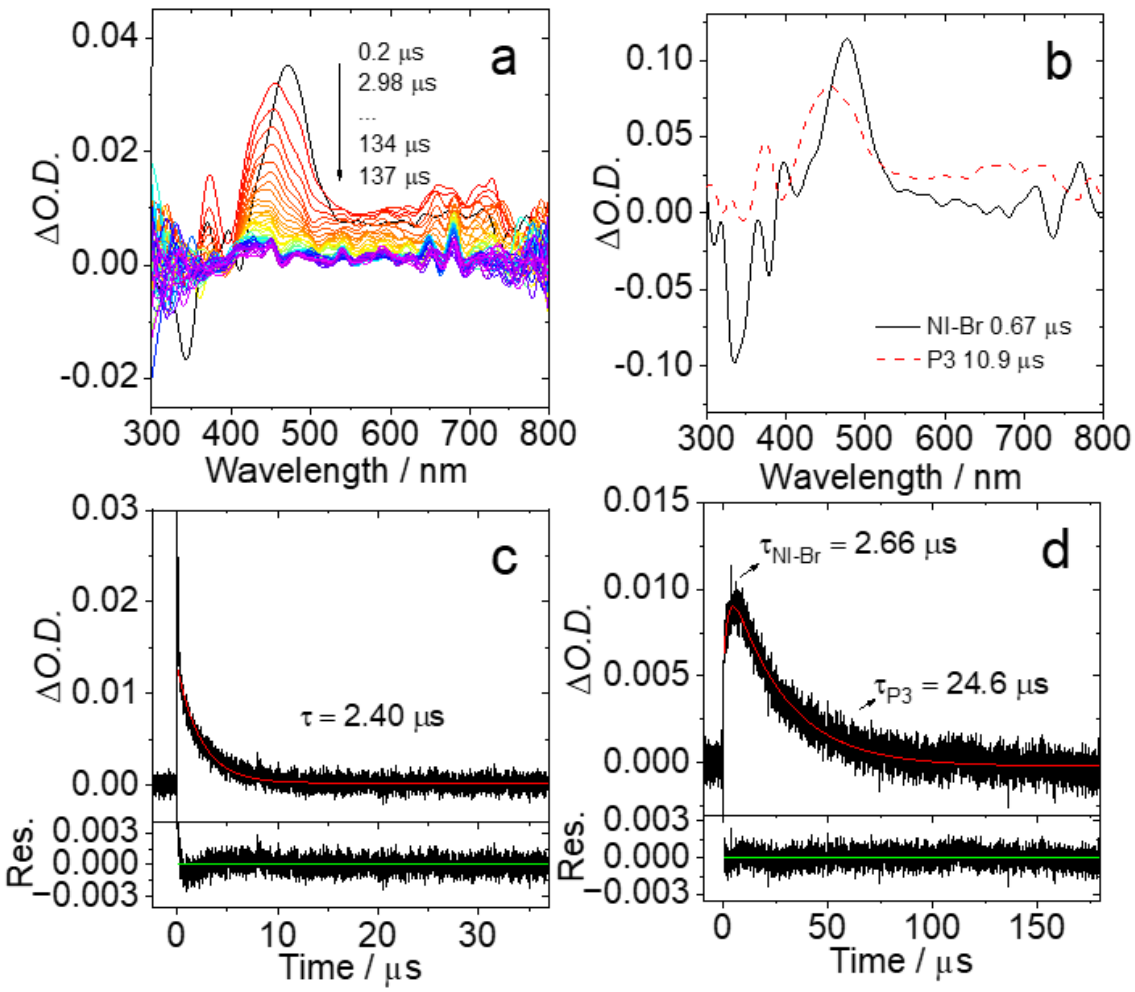

Fig. S38 (a) Intermolecular triplet energy transfer with **NI-Br** as the triplet energy donor and **P1** as the triplet energy acceptor, studied with nanosecond transient absorption spectra. *c* [**P3**] = 2.5 x 10^{-5}M, *c* [**NI-Br**] = 1.0 x 10^{-5}M, λ_{ex} = 355 nm, in deaerated acetonitrile, 25 °C.(b) Species-associated difference spectra (SADS) of the mixture of **NI-Br** with **P3**. The raw data are from (a). Analyzed with global fitting and target analysis. (c) the decay trace at 400 nm. (d) the decay trace at 370 nm.

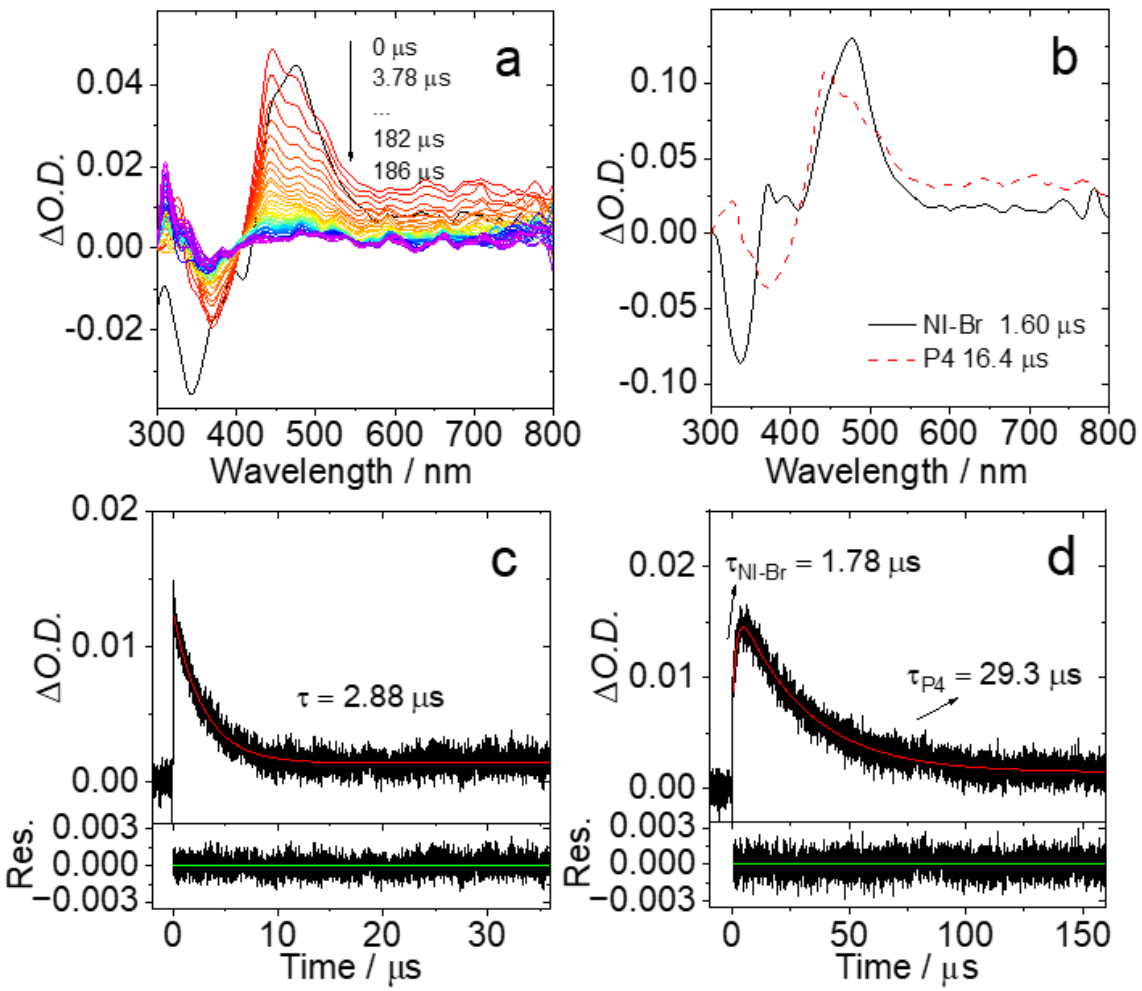

Fig. S39 (a) Intermolecular triplet energy transfer with **NI-Br** as the triplet energy donor and **P4** as the triplet energy acceptor, studied with nanosecond transient absorption spectra. *c* [**P4**] = 2.5 x 10^{-5}M, *c* [**NI-Br**] = 1.0 x 10^{-5}M, λ_{ex} = 355 nm, in deaerated acetonitrile, 25 °C.(b) Species-associated difference spectra (SADS) of the mixture of **NI-Br** with **P4**. The raw data are from (a). Analyzed with global fitting and target analysis. (c) the decay trace at 410 nm. (d) the decay trace at 660 nm.

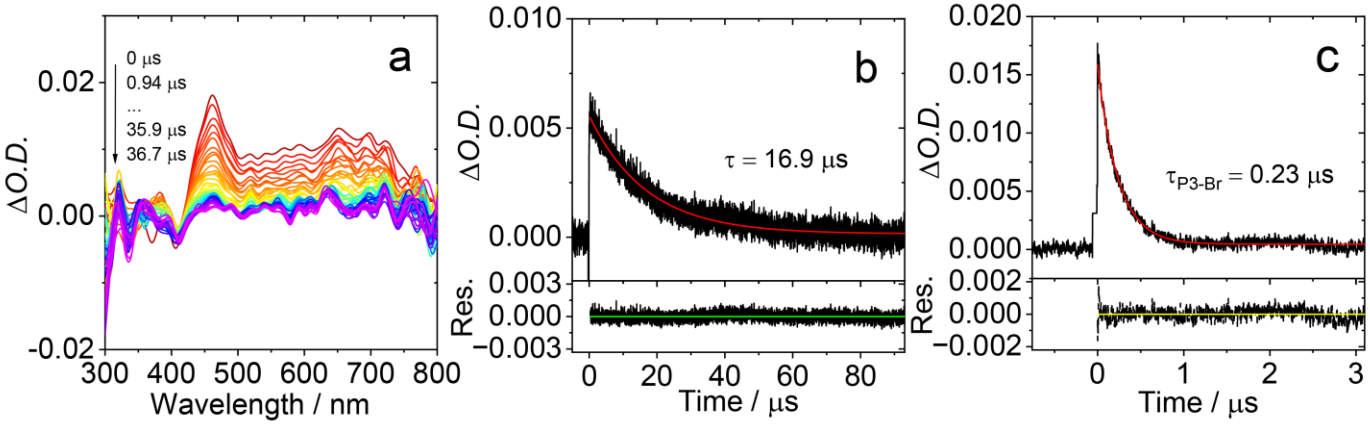

Fig. S40 (a) Nanosecond transient absorption spectra of **P3-Br** and the decay trace at 460 nm in (b) deaerated acetonitrile and (c) aerated acetonitrile. c = 5.0 x 10 $^{-6}$M, λ_{ex} = 355 nm, 25 °C.

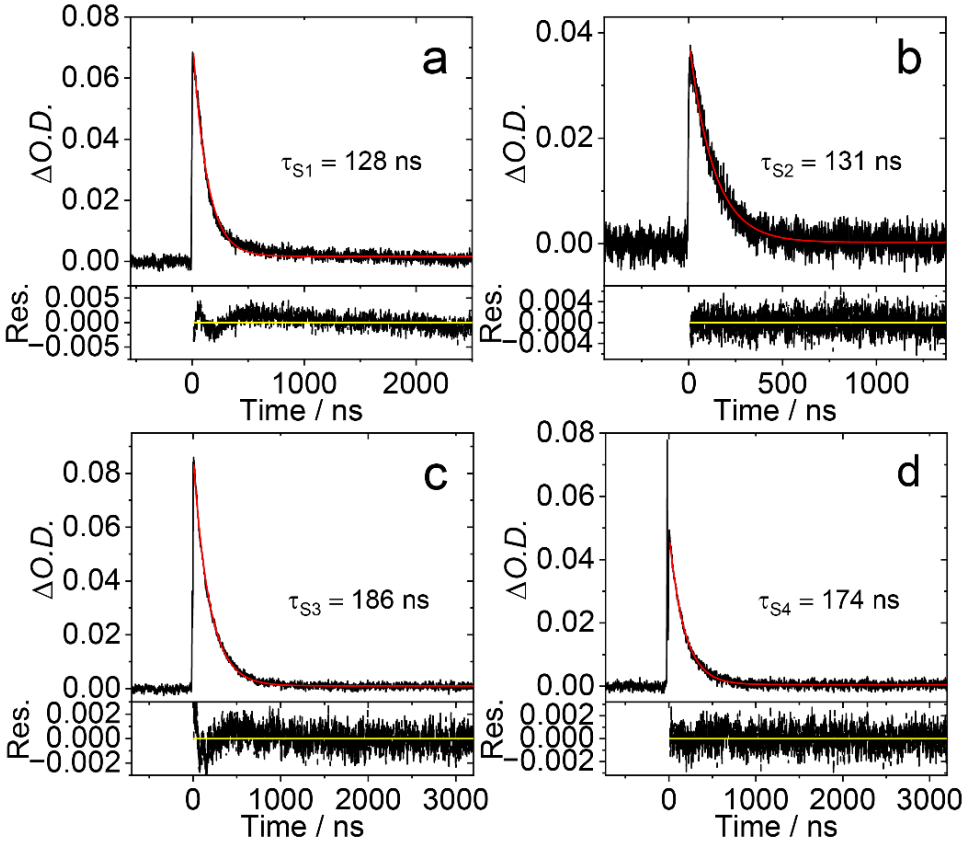

Fig. S41 Nanosecond transient absorption spectra of (a) **S1**, (b) **S2**, (c) **S3**, and (d) **S4**, the decay curves at (a) 610 nm, (b) 700 nm, (c) 510 nm, and (d) 570 nm. c = 1.0 x 10^{-5} M, λ_{ex} = 355 nm, in aerated acetonitrile, 25 °C.

Intrinsic triplet state lifetime fitting: [18]

When the intrinsic triplet state lifetime is long and the triplet state quantum yield is high, the triplet-triplet annihilation will contribute additional lifetime quenching factor to the decay of the transient absorption. Then triplet state lifetime will be quenched significantly and the experimental values will be shorter than the intrinsic lifetime. The corresponding differential equation for the triplet concentration

$$\frac{dC_T}{dt} = -k_1 C_T - k_2 {C_T}^2$$

has the solution:

$$C_T(t) = \frac{c_0 k_1}{\exp(k_1 t)(c_0 k_2 + k_1) - c_0 k_2}$$

Where c0 is the initial triplet concentration. This leads to the following expression for the transient absorption

$$A(t) = \frac{A_0 \tau_2/\tau_1}{\exp(t/\tau_1)(1 + \tau_2/\tau_1) - 1}$$

Where A_0 is the initial transient absorption, $\tau_1 = 1/k_1$ is the intrinsic (unimolecular) lifetime of the triplet, and $\tau_2 = 1/ c_0 k_2$. We fitted the data sets of **P3-Br** triplet state lifetime values simultaneously by Eq. S3, with variation of all parameters (A_0, τ_1, τ_2), but with the intrinsic triplet lifetime constrained to the same value in all data sets.

8. Time-resolved electron paramagnetic resonance (TREPR) spectroscopy

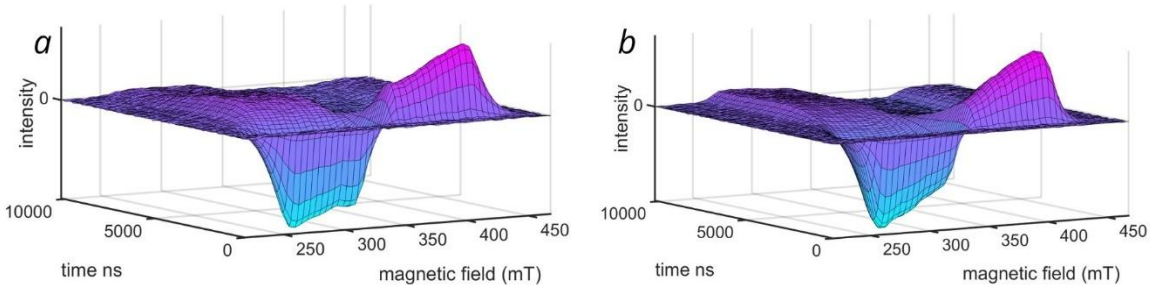

Fig. S42 Experimental TREPR spectra for (a) **S1** (b) **S2**.

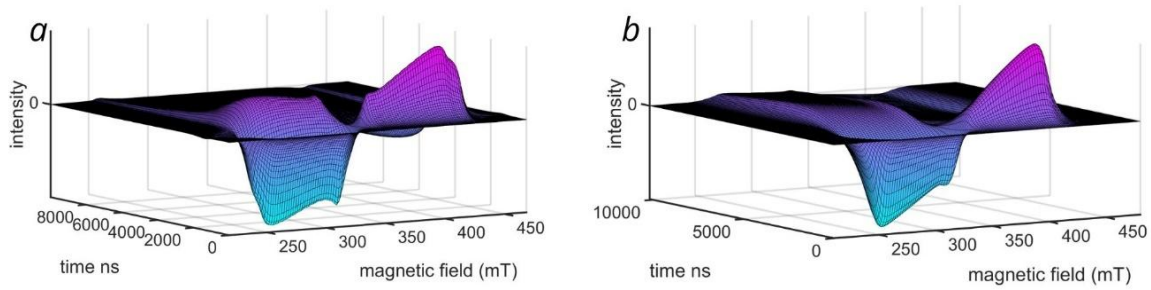

Fig. S43 Simulation spectra (a) **S1** (b) **S2**

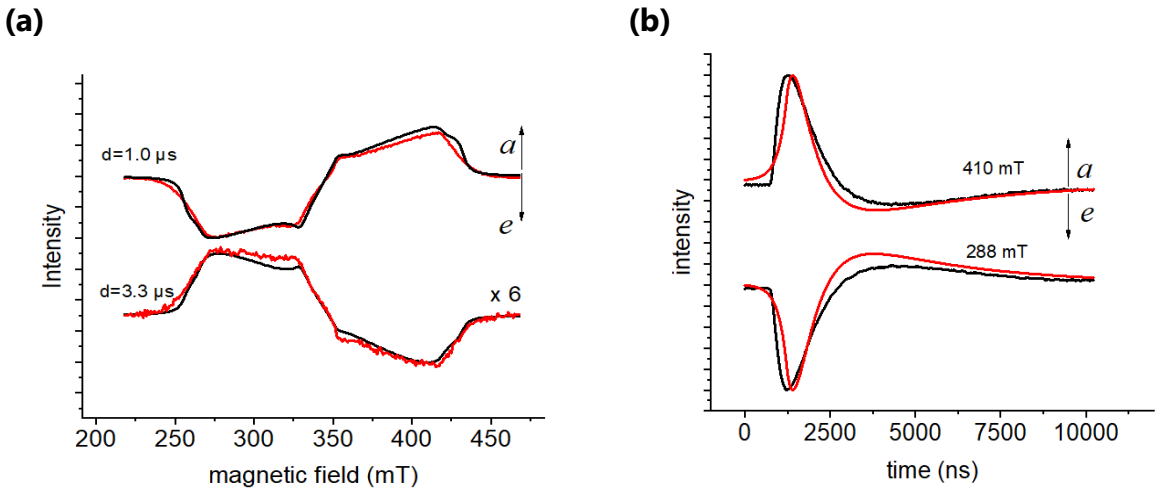

Fig. S44 Slices of the experimental (black) and simulated (red) of the TREPR spectrum of **S1:** (a) spectra along the field and (b) transient signal along the time. The spectra were taken in frozen solution at T = 80 K with pulsed laser at energies of 2.5 mJ/pulse; λ_{ex} = 532 nm, the solvent was TOL/2-MeTHF (3/1, v/v), c=1 × 10^{-3} M.

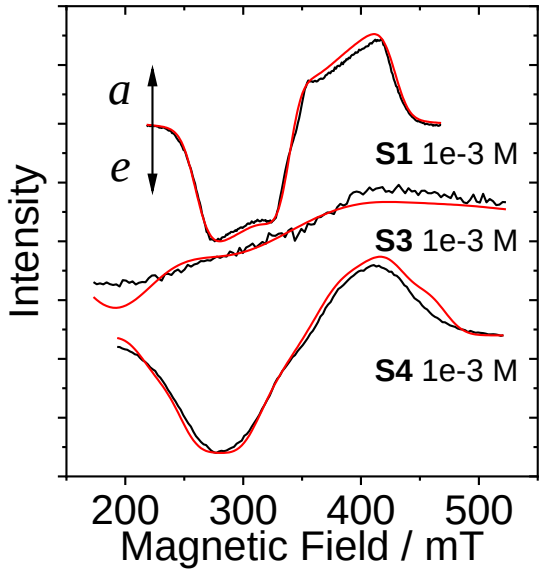

Fig. S45 Experimental TREPR spectra for **S1, S3, S4** after laser excitation, the frozen samples were photo-excited at 532 nm with the pulsed laser at energy of 2.5 mJ and 355 nm with the pulsed laser at energy of 3.2 mJ. **S1, S3, S4** were dissolved in TOL/2-MeTHF (3/1, v/v), c = 1 × 10^{-3} M and the spectra were recorded with frozen solution at 80 K. λ_{ex} = 532 nm for **S1** and **S4**, λ_{ex} = 532 nm for **S3**.

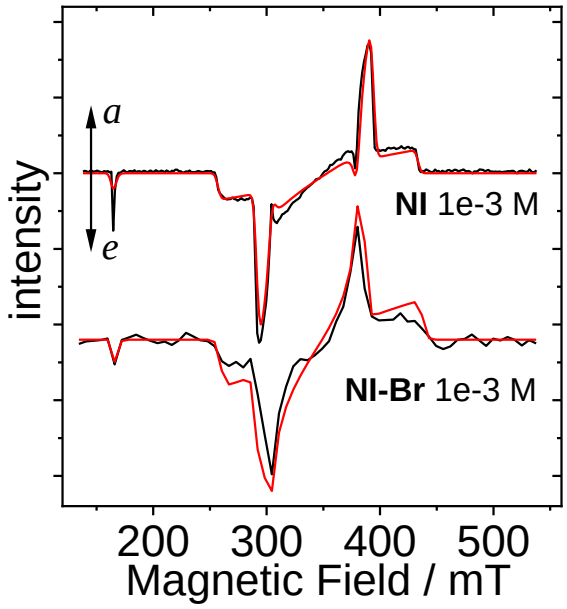

Fig. S46 Experimental TREPR spectra for **NI, NI-Br** after laser excitation, the frozen samples were photo-excited at 355 nm with the pulsed laser at energy of 3.2 mJ. **NI, NI-Br** were dissolved in TOL/2-MeTHF (3/1, v/v), $c = 1 \times 10^{-3}$ M and the spectra were recorded with frozen solution at 80 K.

9. Theoretical Computations.

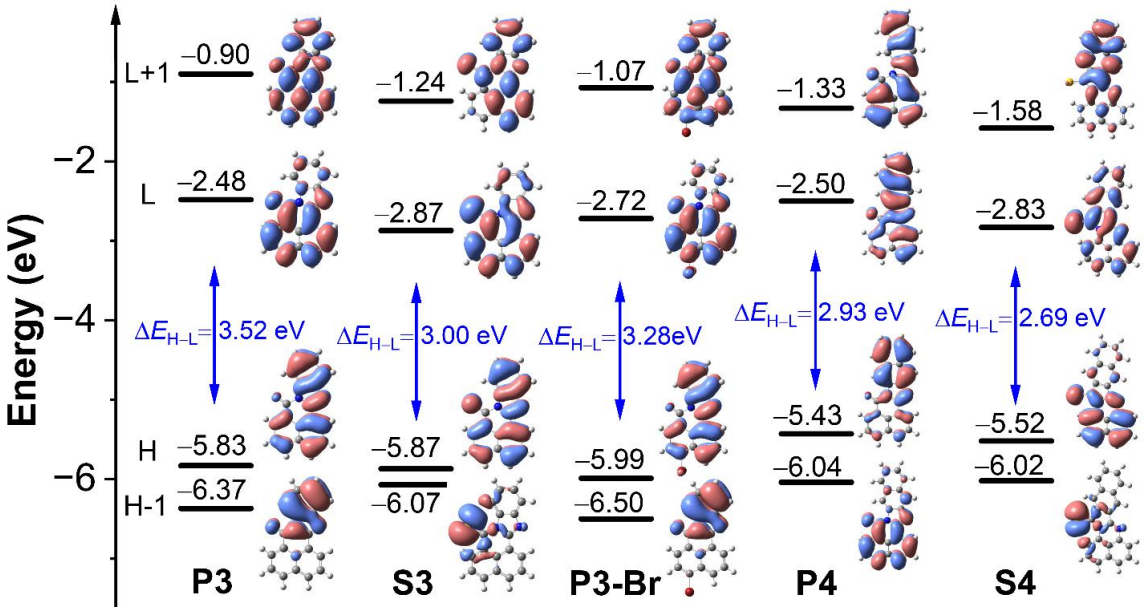

Fig. S47 Selected frontier molecular orbitals of **P3**, **S3**, **P3-Br**, **P4** and **S4** calculated by DFT at the B3LYP/6-31G(d) level with Gaussian 16, based on the optimized ground state in vacuum, respectively (isoval = 0.0004).

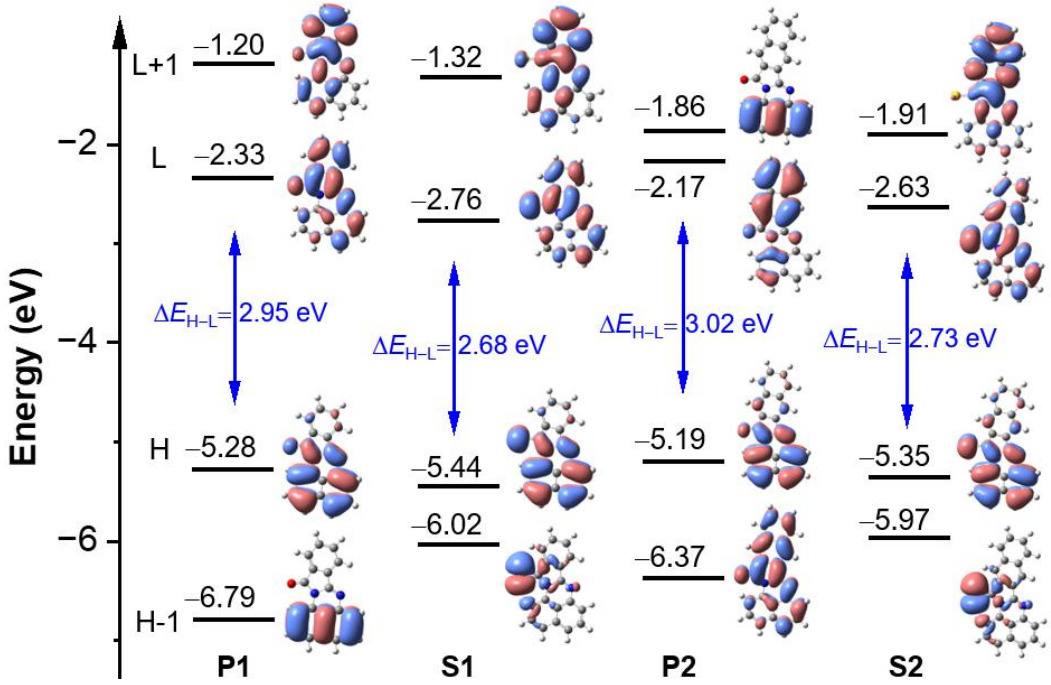

Fig. S48 Selected frontier molecular orbitals of **P1**, **S1**, **P2** and **S2**, calculated by DFT at the B3LYP/6-31G(d) level with Gaussian 16, based on the optimized ground state in vacuum, respectively (isoval = 0.0004).

Table S3. Excitation Energies (eV) and Corresponding Oscillator Strengths (f), Main Configurations, and CI Coefficients of the Low-Lying Electronically Excited States of perinones derivatives and thionated perinones derivatives, performed at the TD-DFT//M06-D3/Def-2-TZVP level by using Gaussian16. Based on optimized ground-state geometries.

	Electronic transition	energy [eV / (nm)][a]	*f*[b]	composition[c]	Configuration Index[d]
S1	$S_0 \rightarrow S_2$	2.57 / 482	0.2834	H→L	0.6905
	$S_0 \rightarrow S_4$	3.63 / 341	0.0603	H–3→L	0.6226
	$S_0 \rightarrow S_6$	3.94 /314	0.0761	H–4→L	0.5678
	$S_0 \rightarrow T_1$	1.55 / 797	0.0000	H→L	0.6854
	$S_0 \rightarrow T_2$	2.08 / 595	0.0000	H–1→L	0.6925
	$S_0 \rightarrow T_3$	2.68 / 530	0.0000	H–2→L	0.5317
S2	$S_0 \rightarrow S_2$	2.53 / 490	0.3801	H→L	0.6859
	$S_0 \rightarrow S_3$	2.92/ 425	0.0127	H→L+1	0.6897
	$S_0 \rightarrow S_4$	3.18 / 389	0.0710	H–2→L	0.6431
	$S_0 \rightarrow T_1$	1.50 / 823	0.0000	H→L	0.6853
	$S_0 \rightarrow T_2$	2.02 / 612	0.0000	H–1→L	0.6931
	$S_0 \rightarrow T_4$	2.43 / 510	0.0000	H–2→L	0.5178
S3	$S_0 \rightarrow S_1$	2.20 / 563	0.0000	H–1→L	0.6903
	$S_0 \rightarrow S_2$	2.74 / 453	0.1787	H–2→L	0.6904
	$S_0 \rightarrow S_4$	3.45 / 359	0.1109	H–3→L	0.6286
	$S_0 \rightarrow T_1$	1.76 / 705	0.0000	H→L	0.6416
	$S_0 \rightarrow T_2$	2.03 / 610	0.0000	H–1→L	0.6838
	$S_0 \rightarrow T_3$	2.44 / 509	0.0000	H–1→L	0.5321
S4	$S_0 \rightarrow S_2$	2.53 / 490	0.2523	H→L	0.6993
	$S_0 \rightarrow S_3$	2.94 / 421	0.0879	H–2→L	0.6822
	$S_0 \rightarrow S_3$	3.59 / 345	0.1168	H→L+1	0.6478
	$S_0 \rightarrow T_1$	1.74 / 714	0.0000	H→L / H–2→L	0.4948 / 0.4088
	$S_0 \rightarrow T_2$	2.06 / 602	0.0000	H–1→L	0.6767
	$S_0 \rightarrow T_3$	2.17 / 570	0.0000	H–2→L	0.4279

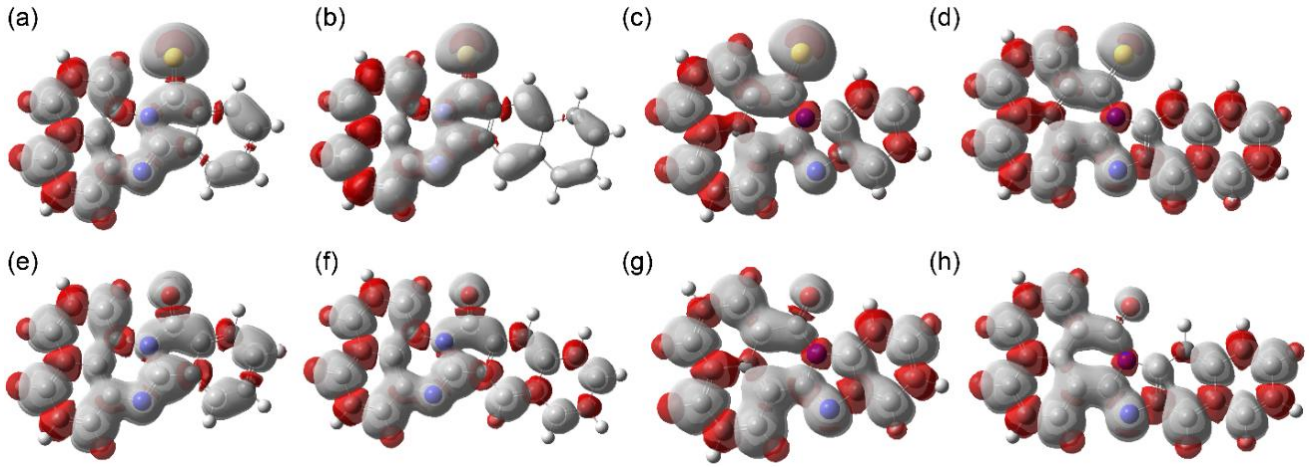

Fig. S49 Spin density surfaces of the T_1 triplet state of (a) **S1**, (b) **S2**, (c) **S3**, (d) **S4**, (e) **P1** (f) **P2** (g) **P3** and (h) **P4** (in gas). Based on the optimized T_1 state geometry. Calculated at the UB3LYP/6-31G(d) level with Gaussian 16 (isoval = 0.0004) in vacuum.

Calculation of the ZFS parameters

Molecular orbitals were calculated using semiempirical AM1 method. The method has proven to give reasonable results in a series of systems. On the other hand, more advanced methods have shown not to perform better. The advantage is in terms of calculation time. The disadvantage is the lack of the calculation of spin/orbit contribution to the ZFS parameters.

Table S4. molecular orbitals calculated by AM1 method.

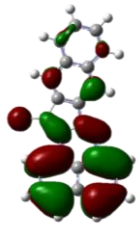	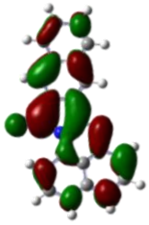	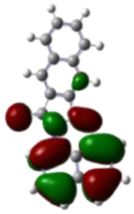	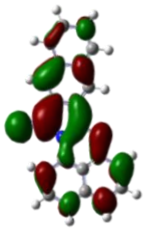	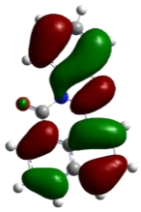	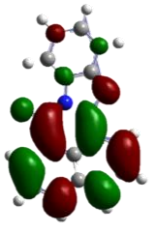
P2 HOMO	LUMO	**S2** HOMO	LUMO	**P3** HOMO	LUMO
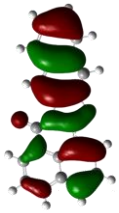	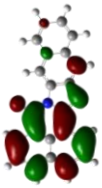	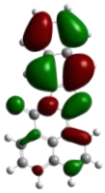	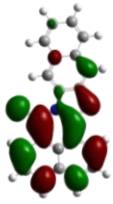	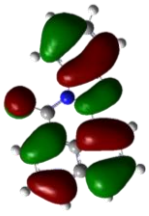	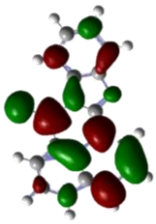
P4 HOMO-1	LUMO	**S4** HOMO	LUMO	**S3** HOMO	LUMO

Table S5. Dipolar contribution to the ZFS parameters as calculated by the point dipolar approximation on AM1-calculated molecular orbitals.

Compounds	*D* (MHz)	*E* (MHz)
P2	2296.4	508.07
S2	2141.7	614.22
P3	2466.9	212.03
S3	2998.2	364.92
P4	755.49	195.37
	2338.5[a]	283.5[a]
S4	777.96	228.44

[a] These values have been obtained using the excited configuration (HOMO-1)–LUMO

Table S6. Decomposition of the triplet-state ZFS parameters into spin–spin and spin–orbit contributions calculated with ORCA (units: cm^{-1}).[a]

Compounds	ZFS		Spin-spin		Spin-orbit	
	D/cm^{-1}	E/cm^{-1}	D/cm^{-1}	E/cm^{-1}	D/cm^{-1}	E/cm^{-1}
P1	0.0135 (–[b])	0.0044 (–[b]	–0.013	0.0208	0.0266	–0.0163
P2	0.0334 (–[b])	0.0045 (–[b])	–0.00044	0.0247	0.0338	–0.02023
P3	–0.0162 (exp 0.078)	–0.0048 (exp 0.01)	–0.0285	0.01182	0.0123	–0.01667
P4	0.0298 (exp 0.06)	0.0064 (exp 0.009)	0.00028	0.02541	0.02950	–0.01902
S1	141.2 (exp 0.077)	0.0831 (exp 0.025)	–0.00438	0.00715	141.1496	0.8062
S2	–3.169 (exp 0.077)	–0.75 (exp 0.021)	0.01196	–0.00417	–818	–0.75
S3	1.595 (exp 0.268)	0.1305 (exp 0.2081)	–0.00785	–0.01704	1.60315	0.22547
S4	–1.876 (exp 0.12)	0.3596 (exp 0.017)	–0.01792	–0.01445	1.8946	0.3742
NI	0.0362 (exp 0.0823[19])	0.0004	–0.0207	0.02496	0.0569	–0.02453
NI-Br	–3.5216 (exp 0.083[20])	0.9117	0.0468	–0.0024	–3.568	–0.9095

[a] The calculation were performed at B3LYP/def2-SVP level using the ORCA 6.1.0 programs[21].
[b] Experimental values are unavailable.

Table S7. SOCMEs (cm^{-1} units) for the State Pairs Evaluated at the Optimized Geometry of the Ground State.[a]

Compound	$T_1 \rightarrow S_0$	$S_1 \rightarrow T_1$	$S_1 \rightarrow T_2$	$S_1 \rightarrow T_3$	$S_1 \rightarrow T_4$	$S_1 \rightarrow T_5$
NI	0	14.98	9.74	0.072	16.55	0.52
NI-Br	0.5	0.07	2.0	0.54	0.04	—
P1	0.02	0	0.01	0.02	0.02	3.87
P2	0.08	0	0.01	0.03	0.05	0.04
P3	0.04	0	0.03	0.01	0.01	0.10
P4	0.08	0.01	0.04	0.01	0.03	0.04
S1	0.22	88.9	0.16	106.61	15.57	4.01
S2	0.20	84.2	0.42	98.5	57.0	13.76
S3	0.28	52.16	0.32	120.3	4.51	48.3
S4	0.15	76.96	0.31	53.7	88.04	21.9

[a] The calculation of the spin orbital coupling matrix elements (SOCMEs) were performed at B3LYP/def2-SVP level using the ORCA 6.1.0 programs[21].

Table S8. Vertical excitation energies for all compounds (eV).[a]

Compound	S_1	S_2	S_3	S_4	T_1	T_2	T_3	T_4	T_5
NI	3.725	3.752	4.040	4.205	2.377	3.392	3.450	3.752	—
NI-Br	3.608	3.681	4.040	4.170	2.316	3.412	3.417	3.665	—
P1	2.905	3.303	3.873	3.881	1.971	2.891	3.037	3.368	3.575
P2	2.557	3.398	3.767	3.814	1.719	2.772	3.068	3.321	—
P3	2.532	3.020	3.581	3.763	1.836	2.411	2.600	2.999	3.340
P4	2.591	2.825	3.587	3.826	1.806	2.324	2.753	3.023	3.133
S1	2.144	2.576	3.055	3.321	1.656	1.844	2.217	2.746	3.129
S2	2.212	2.466	3.369	3.476	1.414	1.884	2.567	2.799	3.011
S3	2.167	2.339	2.777	3.286	1.649	1.877	1.952	2.413	2.724
S4	2.277	2.496	2.834	3.164	1.515	1.949	2.264	2.392	—

[a] Calculated by DFT at the TD-DFT//M06-D3/Def-2-TZVP level using Gaussian 16. In gas phase.

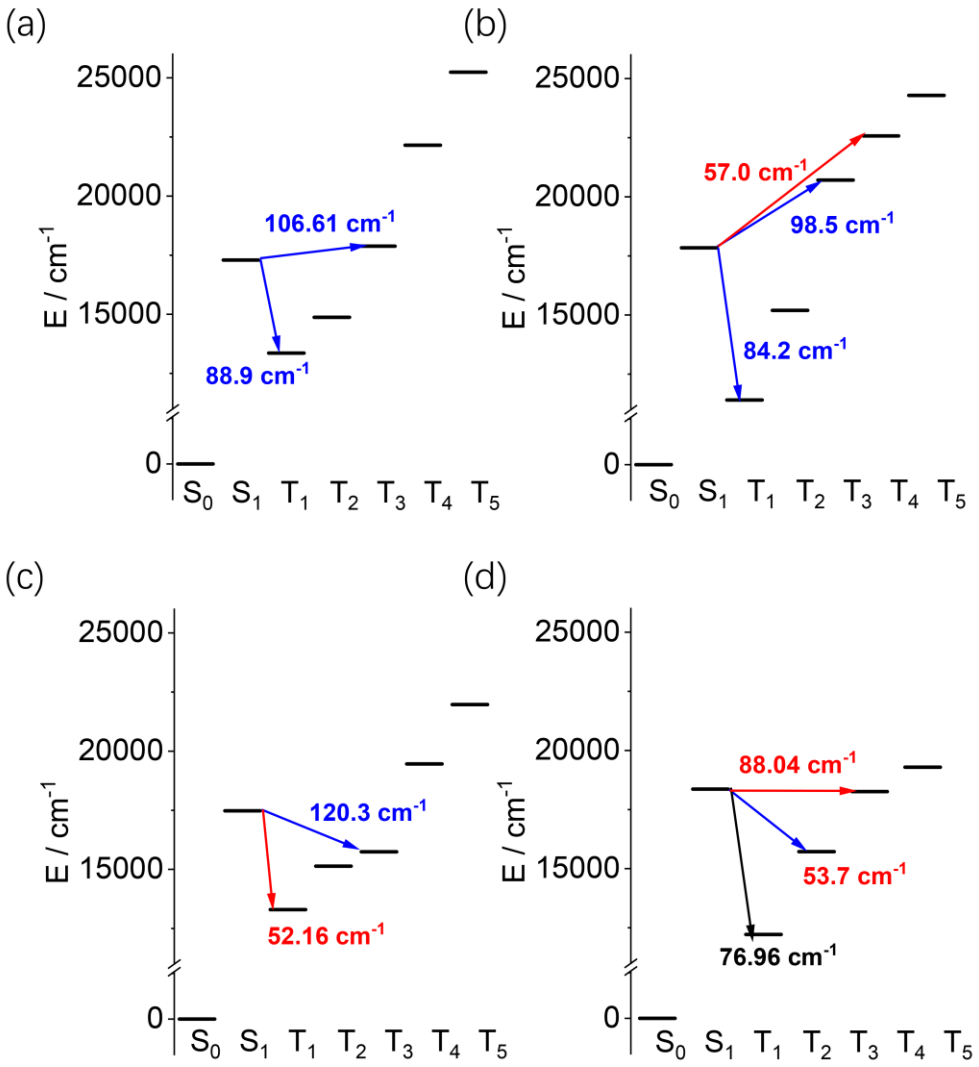

Fig. S50 ISC energy-level diagrams of thionated perinones **S1**–**S4**. Energies (cm^{-1}) are converted from TDDFT vertical excitation energies (Table S8; 1 eV = 8065.54 cm^{-1}). Arrows indicate the two selected $S_1 \rightarrow T_n$ ISC channels; numbers are SOCMEs (cm^{-1}) from Table S7. (a) **S1**, (b) **S2**, (c) **S3** and (d)**S4**.

10. References

[1] J. J. Snellenburg, S. Laptenok, R. Seger, K. M. Mullen and I. H. M. van Stokkum, *Glotaran: A Java-Based Graphical User Interface for the R Package TIMP*, 2012. *J. Stat. Softw.*, 2012, **49**, 1–22.

[2] S. Stoll and A. Schweiger, *J. Magn. Reson.*, 2006, **178**, 42–55.

[3] T. Hatakeyama, K. Shiren, K. Nakajima, S. Nomura, S. Nakatsuka, K. Kinoshita, J. Ni, Y. Ono and T. Ikuta, *Adv. Mater.* 2016, **28**, 2777–2781.

[4] M. J. Frisch, G. W. Trucks, H. B. Schlegel, G. E. Scuseria, M. A. Robb, J. R. Cheeseman, G. Scalmani, V. Barone, G. A. Petersson, H. Nakatsuji, X. Li, M. Caricato, A. V. Marenich, J. Bloino, B. G. Janesko, R. Gomperts, B. Mennucci, H. P. Hratchian, J. V. Ortiz, A. F. Izmaylov, J. L. Sonnenberg, Williams, F. Ding, F. Lipparini, F. Egidi, J. Goings, B. Peng, A. Petrone, T. Henderson, D. Ranasinghe, V. G. Zakrzewski, J. Gao, N. Rega, G. Zheng, W. Liang, M. Hada, M. Ehara, K. Toyota, R. Fukuda, J. Hasegawa, M. Ishida, T. Nakajima, Y. Honda, O. Kitao, H. Nakai, T. Vreven, K. Throssell, J. A. Montgomery Jr., J. E. Peralta, F. Ogliaro, M. J. Bearpark, J. J. Heyd, E. N. Brothers, K. N. Kudin, V. N. Staroverov, T. A. Keith, R. Kobayashi, J. Normand, K. Raghavachari, A. P. Rendell, J. C. Burant, S. S. Iyengar, J. Tomasi, M. Cossi, J. M. Millam, M. Klene, C. Adamo, R. Cammi, J. W. Ochterski, R. L. Martin, K. Morokuma, O. Farkas, J. B. Foresman and D. J. Fox, *Gaussian 16 Rev. C.01, Wallingford, CT,* 2016.

[5] Y. L. Niu, Q.A. Peng, C.M. Deng, X. Gao, Z.G. Shuai, *J. Phys. Chem. A* 2010, **114**, 7817–7831.

[6] M. Etinski, J. Tatchen, C.M. Marian, *J. Chem. Phys.* 2011, **134**, 154105.

[7] M. Etinski, V. Rai-Constapel, C.M. Marian, *J. Chem. Phys.* 2014, **140**, 114104.

[8] M. Etinski, J. Tatchen, C.M. Marian, *Phys. Chem. Chem. Phys.* 2014, **16**, 4740–4751.

[9] A. Baiardi, J. Bloino, V. Barone, *J. Chem. Theory. Comput.* 2013, **9**, 4097–4115.

[10] B. de Souza, F. Neese, R. Izsak, *J. Chem. Phys.* 2018, **148**, 034104.

[11] F. Neese, F. Wennmohs, U. Becker, C. Riplinger, *J. Chem. Phys.* 2020, **152**, 224108.

[12] F. Neese, Software update: the ORCA program system, version 5.0, *WIRES Comput. Molec. Sci.* 2022, **12**, e1606.

[13] B. de Souza, G. Farias, F. Neese, R. Izsak, *J. Chem. Theory Comput*. 2019, **15**, 1896–1904.

[14] J. R. Palmer, K. A. Wells, J. E. Yarnell, J. M. Favale and F. N. Castellano, *J. Phys. Chem. Lett.*, 2020, **11**, 5092–5099.

[15] T. C. Pham, S. Heo, V.-N. Nguyen, M. W. Lee, J. Yoon and S. Lee, *ACS Appl. Mater. Interfaces*, 2021, **13**, 13949–13957.

[16] J.-F. Lee and S. L.-C. Hsu, *Polymer*, 2009, **50**, 5668–5674.

[17] N. Campbell, W. W. Easton, J. L. Rayment and J. F. K. Wilshire, *J. Chem. Soc.*, 1950, 2784–2787.

[18] Z. Wang, A. A. Sukhanov, A. Toffoletti, F. Sadiq, J. Zhao, A. Barbon, V. K. Voronkova and B. Dick, *J. Phys. Chem. C*, 2019, **123**, 265–274.

[19] X. Zhang, Z. Xu, A. A. Sukhanov, X. Yang, A. Elmali, J. Zhao, B. Dick, A. Karatay and V. K. Voronkova, *Org. Chem. Front.*, 2025, **12**, 3344–3362

[20] K. Chen, I. V. Kurganskii, X. Zhang, A. Elmali, J. Zhao, A. Karatay, M. V. Fedin, *Chem. Eur. J.*, 2021, **27**, 7572–7587.

[21] F. Neese, *WIREs Comput. Mol. Sci.,* 2025, **15**, e70019.